Independent Components of Magnetoencephalography: Localization and Single-Trial Response Onset Detection

Akaysha C. Tang Barak A. Pearlmutter

Abstract

Independent component analysis (ICA) is a class of decomposition methods that separate sources from mixtures of signals. In this chapter, we used second order blind identification (SOBI), one of the ICA method, to demonstrate its advantages in identifying magnetic signals associated with neural information processing. Using 122-channel MEG data collected during both simple sensory activation and complex cognitive tasks, we explored SOBI's ability to help isolate and localize underlying neuronal sources, particularly under relatively poor signal-to-noise conditions. For these identified and localized neuronal sources, we developed a simple threshold-crossing method, with which single-trial response onset times could be measured with a detection rate as high as 96%. These results demonstrated that, with the aid of ICA, it is possible to non-invasively measure human single trial response onset times with millisecond resolution for specific neuronal populations from multiple sensory modalities. This capability makes it possible to study a wide range of perceptual and memory functions that critically depend on the timing of discrete neuronal events.

The goal of this chapter is to introduce the basic concept of independent component analysis (ICA), a class of algorithms that decompose a multidimensional time series into a set of components, each with a one-dimensional time course and a fixed spatial distribution. For magnetoencephalography (MEG) as well as electroencephalography (EEG), the multidimensional time series corresponds to the multichannel MEG or EEG recordings, the component time series to simultaneously separated and temporally overlapping signals from various neuronal populations, and the spatial distributions to the set of attenuations from the neuronal sources to the sensors. While the component time series provides temporal information about the evoked neuronal responses and ongoing activity, the sensor projection vectors give information about the spatial locations of the neuronal sources.

One particular ICA algorithm, the second order blind identification (SOBI) (Belouchrani et al., 1993; Cardoso, 1994) will be used as an example to illustrate the procedures for separating the mixture of noise and neuromagnetic signals into neurophysiological and neuroanaotmically meaningful components, for localizing their corresponding source generators, and for measuring single-trial response onset times from the localized neuronal populations. Systematic comparisons between SOBI and alternative ICA algorithms (*e.g.*, InfoMax (Bell and Sejnowski, 1995) and fICA (Hyvärinen and Oja, 1997)) using the same data set remain to be conducted.

The chapter is organized into six parts.

- Part one defines the ICA problem and offers the reader considerations in selecting a specific ICA algorithm. Second order blind identification (SOBI), will be introduced as our algorithm of choice for separation of MEG data. The relationship between ICA and other decomposition and source localization methods will be briefly discussed.

- Part two discusses the task conditions under which ICA is most likely to be beneficial, specifically low S/N conditions resulting from large trial-to-trial variability and small number of trials in behavioral tasks. The behavioral tasks used in this chapter will be described.

- Part three describes the process of SOBI application to neuromagnetic signals. SOBI components will be characterized in both time and space using *MEG images* and *field maps* respectively. A variety of common neuronal and non-neuronal SOBI components will be identified using both temporal and spatial information as constraints.

- Part four describes the process of finding equivalent current dipole models for SOBI neuronal components. The time-invariance of a SOBI component's field map and the resulting reduction in the subjectivity of localization process will be discussed. Cross-task and cross-subject reliability will be examined. Systematic comparisons between source localizations with and without the aid of SOBI will be made.

- Part five describes the process of detecting single-trial response onset times in SOBI separated neuronal components. An iterative threshold-crossing method will be used in measuring single-trial response onset times. Examples of onset time detection will be provided for three major sensory modalities. Cross-subject reliability will be demonstrated for each of three major sensory modalities.

- Part six summarizes capabilities and advantages that SOBI offers to the analysis of MEG data and discusses assumptions and future directions.

We assume that the readers have a basic knowledge of MEG and the standard analysis tools offered by commercially available Neuromag software. Comprehensive reviews on ICA algorithms will be avoided due to space limitation. For reviews of ICA see Amari and Cichocki (1998); Cardoso (1998); Hyvärinen (1999); Vigário et al. (2000).

1 Introduction

1.1 ICA: Definition

Let $\mathbf{x}(t)$ be an n-dimensional vector of sensor signals, which we assume to be an instantaneous linear mixture of n unknown independent underlying components $s_i(t)$, *via* the unknown $n \times n$ mixing matrix $\mathbf{A}$,

$$\mathbf{x}(t) = \mathbf{A}\,\mathbf{s}(t) \tag{1}$$

The ICA problem is to recover $\mathbf{s}(t)$, given the measurements $\mathbf{x}(t)$ and nothing else. This is accomplished by finding a matrix $\mathbf{W}$ which approximates $\mathbf{A}^{-1}$.

For MEG, $x_i(t)$ corresponds to either continuous or averaged sensor readings from a magnotometer or gradiometer and $s_i(t)$ to a recovered neuronal or noise source. n is the number of sensors available. ICA decomposes the mixed sensor signals $\mathbf{x}(t)$ into n components.

The output of the algorithm is a $n \times n$ matrix, $\mathbf{W}$, which maps from the vector of sensor values $\mathbf{x}(t)$ to the vector of recovered component values $\hat{\mathbf{s}}(t) = \mathbf{W}\,\mathbf{x}(t)$ (Fig. 1), up to a scaling and permutation of the components.

The types of true sources that affect MEG sensor readings are summarized on the left side of Fig. 1. When ICA does a good job, the recovered components $\hat{\mathbf{s}}(t)$ correspond to the true sources.

1.2 ICA Components in Time

The recovered components $\hat{\mathbf{s}}_i(t)$ can be displayed as a plot of signal strength as a function of time, or alternatively in an *MEG image* (*e.g.* Fig. 4 right), a pseudo-colored bitmap in which the responses of a given component during an entire experiment can be parsimoniously displayed (Jung et al., 1999b). Typically, each row represents one discrete trial of stimulation and multiple trials are ordered vertically from top to bottom. MEG images can be very informative in providing not only averaged but trial-to-trial temporal information about the source activation, such as the single-trial response onset times of a given separated component. For exam-

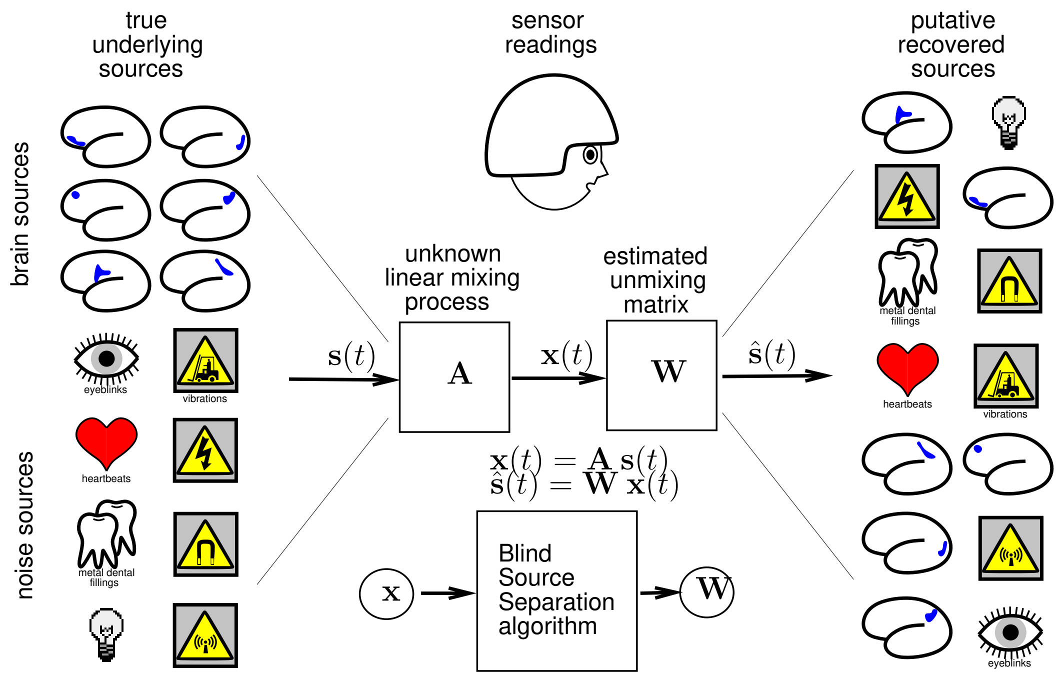

Figure 1: The ICA process. Signals from the brain and other noise sources $\mathbf{s}(t)$ are mixed through an unknown linear mixing process $\mathbf{A}$, resulting in the sensor readings $\mathbf{x}(t) = \mathbf{A}\mathbf{s}(t)$. ICA finds an unmixing matrix $\mathbf{W}$ that maps from the sensor signals to recovered components $\hat{\mathbf{s}}(t) = \mathbf{W}\mathbf{x}(t)$. The entries of the attenuation matrix $\mathbf{A} = \mathbf{W}^{-1}$ describe how strongly each sensor responds to each component.

ples of MEG images of noise sources see Fig. 4 right and of neuronal sources, see Fig. 12b, Fig. 13cd, and Fig. 14b.

1.3 ICA Components in Space

Although ICA does not assume any physical model of the neuronal source generators, spatial information concerning a separated component is given by the *field map* of the component, which represents the measured *sensor* response to the activation of the component $\hat{s}_i(t)$. In other words, the field map of a neuronal component gives the sensor readings when the corresponding neuronal *source* alone is activated. Examples of field maps for a visual, somatosensory, and auditory components are shown in Fig. 5b. The field map of the i^{th} component $\hat{s}_i(t)$ is the i^{th} column of the estimated attenuation matrix $\hat{\mathbf{A}}$, where $\hat{\mathbf{A}} = \mathbf{W}^{-1}$. In combination with the structural MRI, the field maps can be used as input to any localization tools for localizing the separated components within the brain. For example, after calculating its sensor projection, we can repackage a component for localization by Neuromag dipole modeling tools.

1.4 Selection of ICA Methods

ICA algorithms (for review, see Amari and Cichocki (1998); Cardoso (1998); Hyvärinen (1999); Vigário et al. (2000)) fall between two extremes: instantaneous and summary algorithms, that differ in whether each point in time is considered in isolation. Instantaneous algorithms (such as Bell-Sejnowski Infomax and fICA) make repeated passes through the dataset to update the unmixing matrix in response to the data at each time-point. Signals are assumed to have no temporal correlation, and the results are meant to be invariant to shuffling of the data. In contrast, summary algorithms, such as SOBI (Belouchrani et al., 1993; Cardoso, 1994), first make a pass through the data while summary statistics are accumulated by averaging; they then operate solely upon the summary statistics to find the separation matrix.

In selection of ICA algorithms for MEG applications, one important consideration is the robustness of the algorithm to noise. In general, summary algorithms are more likely to be less sensitive to noise because their summary statistics are averages over time. The relatively poor signal-to-noise ratio in MEG data suggests the choice of a summary algorithm, such as SOBI, over an instantaneous algorithm. When it can be assumed that each source has a broad autocorrelation function, as is the case with brain signals, SOBI can give high quality separation while imposing rather modest computational requirements.

SOBI extracts a large set of statistics from the dataset, which it uses for the separation. Each of these statistics is calculated by averaging across the dataset, which makes the algorithm robust against noise. The particular statistics calculated are the correlations between pairs of sensors at a fixed delay, $\langle x_i(t)x_j(t+\tau)\rangle$. This makes good use of abundant but noisy data, and most importantly, SOBI can be tuned by modifying its set of delays, allowing its users to gently integrate a very weak form of prior knowledge.

1.5 Second Order Blind Identification

SOBI is considered blind as it makes no assumptions about the form of the mixing process. In other words, *SOBI does not attempt to solve the inverse problem* or use the physics of the situation in any way. It does not try to estimate currents, or know about Maxwell's equation or any of its consequences. The only physical assumption made about the mixing process is that it is instantaneous and linear.

As stated before, the ICA problem is to recover $\mathbf{s}(t)$, given the measurements $\mathbf{x}(t)$ and nothing else. This is accomplished by finding a matrix $\mathbf{W}$ which approximates $\mathbf{A}^{-1}$, up to permutation and scaling of its rows. SOBI assumes that the components are statistically independent in time, and not necessarily orthogonal in space. It finds $\mathbf{W}$ by minimizing the total correlations between one component at time t and another at time $t + \tau$, computed with a set of time delays (τs) [1]

The particular set of delays τ can be chosen to cover a reasonably wide interval without extending beyond the support of the autocorrelation function. Measured in units of samples at a 300 Hz sampling rate, a reasonable set of delays is

$$\begin{aligned}\tau \in \{ \; & 1, 2, 3, 4, 5, 6, 7, 8, 9, \\ & 10, 12, 14, 16, 18, \\ & 20, 25, 30, 35, 40, 45, 50, 55, \\ & 60, 65, 70, 75, 80, 85, 90, 95, 100 \; \}.\end{aligned}$$

It is important to point out that the choice of delays can affect the results of separation. Depending on the types of sources activated by the behavioral task, the selection of delays can have complex interactions with the latency of evoked responses. Prior knowledge about the sources can be incorporated by setting these parameters.

1.6 ICA versus Other Decomposition Methods

Both PCA (Hotelling, 1933) and ICA (Comon, 1994) can be thought of as decomposing the matrix whose rows are the sensor values at various points in time into a sum of rank-one matrices. Each of these rank-one matrices is an outer product of two vectors: one representing a time course, the other a set of spatial attenuations. The question is: what is the best decomposition. PCA assumes that the data is Gaussian and requires the vectors that form the outer products to be *orthogonal*, while ICA models the data as generated by *statistically independent* but *non-Gaussian* processes.

Jung et al. (1999a) applied both PCA and ICA to EEG data and assessed their ability to segregate various known sources of noise. They found that ICA was superior in this regard. Vigário et al. (1999) applied both methods to MEG data and the auditory and somatosensory ICA components were physiologically more reasonable than the PCA components. These results are not surprising, given the poor match between PCA's assumptions (Gaussian, orthogonal) and the actual processes generating the data (highly non-Gaussian, highly correlated spatial attenuations.)

[1] For justification for this minimization, see Sec 6.1.

1.7 ICA and Other Source Modeling Methods

Beside ICA, a variety of algorithms have been developed (Mosher et al., 1992; Ioannides et al., 1995; Kinouchi et al., 1996; Sekihara et al., 1997; Nagano et al., 1998; Mosher and Leahy, 1998; Uutela et al., 1998; Mosher and Leahy, 1999; Schwartz et al., 1999; Sekihara et al., 2000; Huang et al., 2000; Aine et al., 2000; Ermer et al., 2000; Schmidt et al., 1999) to localize neuronal sources or to simultaneously localize and recover the time course of these neuronal sources from a mixture of source signals recorded at multiple sensors. Because ICA can generate sensor projections of functionally independent components, ICA can be viewed, not as an alternative to existing source modeling method, but as a pre-processing tool that generate "cleaner" sensor readings from functionally unique neuronal populations. Given their ability to separate the noise from neuronal signals, ICA algorithms are expected to benefit all source localization methods by providing them with input signals that are more likely to be associated with functionally independent neuronal sources.

1.8 ICA and MEG

Application of ICA to MEG was preceded by its application to EEG five years ago (Makeig et al., 1996). Since then, several independent component analysis (ICA) algorithms, such as second-order blind identification (SOBI) (Belouchrani et al., 1993; Cardoso, 1994), Bell and Sejnowski (1995) Infomax, and fast independent component analysis (fICA) (Hyvärinen and Oja, 1997), have been applied to EEG data (Makeig et al., 1997, 1999; Jung et al., 2000a,b) and MEG data (Vigário et al., 1998; Tang et al., 2000a,b; Vigário et al., 1999, 2000; Wübbeler et al., 2000; Ziehe et al., 2000; Cao et al., 2000). In both applications, ICA methods have proven useful for artifact removal (Jung et al., 2000a,b; Vigário et al., 1998; Tang et al., 2000a; Ziehe et al., 2000). Neurophysiologically meaningful components have been separated (Makeig et al., 1997, 1999; Vigário et al., 1999; Tang et al., 2000a; Wübbeler et al., 2000; Tang et al., 2002a,b). For MEG, these neurophysiologically meaningful ICA components have been further localized using equivalent current dipole models (Vigário et al., 1999; Tang et al., 2000c). Most recently, single-trial response onset times have been estimated with an over 90% success rate from these functional components (Tang et al., 2002a).

2 When to Use ICA?

Typical magnetic signals associated with neuronal activity are on the order of one hundred fT, while the noise signals within a shielded room tend to be much larger (Lewine and Orrison, 1995). Furthermore, the intrinsic sensor noise is comparable in magnitude to some small neuronal signals. Therefore, what the sensors record during an experiment is always a mixture of small neuromagnetic and large noise signals. This poor signal-to-noise ratio[2] can affect the estimation of temporal profile and localization of neuronal activity.

Because one strength of ICA is its ability to separate various noise sources from the signals of interest, ICA is most likely to be useful when the experimental conditions necessitate relatively poor S/N. For example, the somatosensory responses associated with thumb mouse-button presses without any constrains on the resting position of the hand and on how the hands holding the mouse would have a relatively poor S/N while somatosensory responses associated with well-controlled median nerve stimulation would have a much higher S/N. If more or few trials of stimulation are conducted, the S/N in the average responses can be higher or lower accordingly. ICA is expected to be particularly useful when a small number of trials of data were collected, when the behavioral tasks involve large variability in stimulus presentation or behavioral responses requirement, when neuronal sources of interests lie beyond the early sensory processing areas, and when the tasks are highly cognitive in contrast to sensory activation tasks. Therefore, ICA may support experimental designs that more closely approximate perceptual, motor, and cognitive processing taking place in the real world.

As the details of the behavioral tasks are critical in assessing the utility of ICA, we briefly describe the tasks used in generating the data for the following ICA application. We collected MEG data from four subjects during four visual reaction time tasks, originally designed for studying temporal lobe memory (Tang et al., 2002a,b). In each task, a pair of colored patterns was presented on the left and right halves of the display screen. The subject was instructed to press either the left or right button when the target appeared on the left or right, respectively. In all tasks, the target was not described to the subject prior to the experiment. The subject was to discover the target by trial and error using auditory feedback (low and high tones corresponded to correct and incorrect responses, respectively). All subjects were able to discover the rule within a few trials.

The tasks differed in the memory load required for determining which of the

[2]Unless otherwise indicated, we use signal-to-noise ratio in the sense defined in signal detection theory. Signals refer to the neuromagnetic signal of interest. Noise refers to all other signals including environmental and sensor noise and other background brain signals.

pair is the target. Task one served to familiarize the subjects with all visual patterns. The subjects simply viewed the stimuli and were asked to press either the left or right button at their own choice while making sure approximately equal numbers of left and right button presses were performed. As such, task one placed little memory demand on the subject. Task two involved remembering a single target pattern which appeared on each trial paired with other patterns. Subjects were to press the corresponding button to indicate the side of the screen on which the target pattern was displayed. Task three involved remembering multiple targets, each always paired with the same non-targets. Task four was the most complex, in which whether a pattern was a target was context sensitive as in the game of rock-paper-scissors. The amount of cognitive processing beyond the initial sensory processing increased from task one to task four.

We used data from these complex cognitive tasks to evaluate the capability of SOBI because of the relatively poor signal-to-noise ratios involved in comparison to simple sensory activation tasks. Specifically, these tasks involved (1) large visual field stimulation without the use of fixation points, (2) incidental somatosensory stimulation as a result of button presses during reaction time tasks, and (3) highly variable button press responses because precisely what form of the thumb movement should be made, how the mouse was held, and where the hands rest were not specified. These sources of variability in visual and somatosensory activation can lead to poor signal-to-noise ratios in the average responses, making it particularly difficult to localize the neuronal sources from unprocessed averaged sensor data. In addition, the involvement of higher level cognitive functions, memory demand, and the small number of trials collected under each task condition, 90 trials in most cases, could further decrease the signal-to-noise ratio in the average sensor data. As such, these tasks offer challenging cases in which the unique advantages of ICA methods may be revealed.

To include data from high signal-to-noise experimental conditions, data from a separate *auditory sensory activation task* (binaural 500 Hz tone, 200 ms duration, 3.25 ± 0.125 ms SOA, 150 trials) will also be used. Together, these tasks offer data collected under both poor and good signal to noise conditions (cognitive tasks: poor; sensory activation task: good) and data involving activation of neuronal sources from three major sensory modalities.

3 Identification of SOBI Neuronal Components

Using SOBI, continuous MEG signals from 122 channels were separated into 122 components. Each of the components has a time course, which can be averaged across multiple trials using either the visual stimulus onset or the button press as

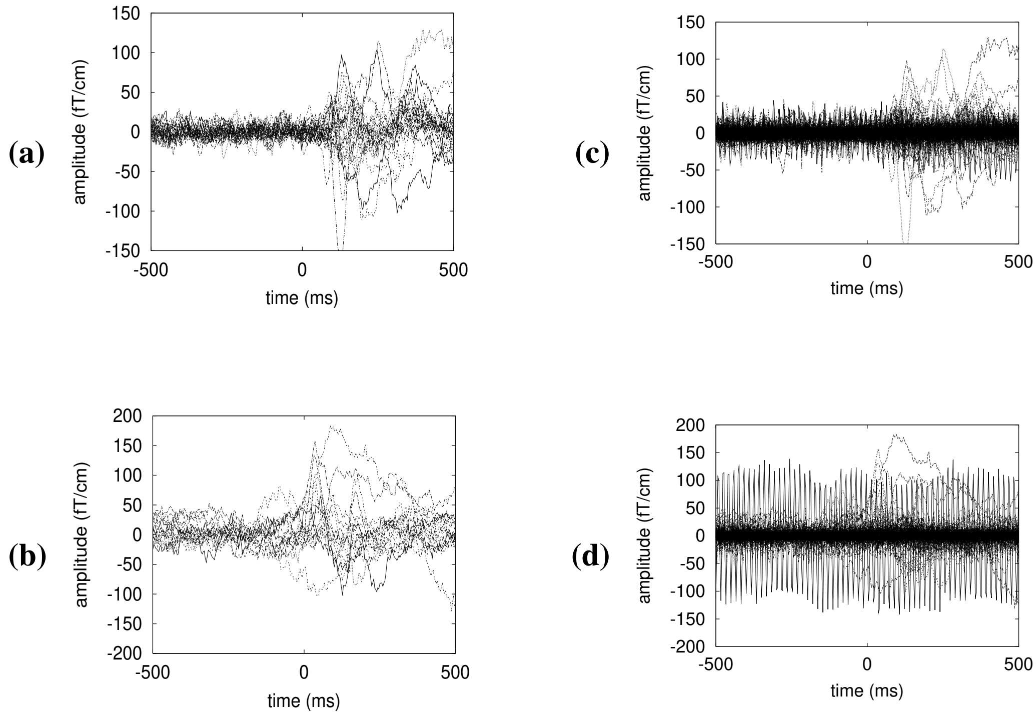

Figure 2: Event-triggered averages for groups of SOBI components ($N = 90$ trials). **(a)** Components showing visual-stimulus-triggered responses, triggered on visual stimulus onset. **(b)** Components showing button-press-triggered responses, triggered on button presses. **(c)** All components, triggered on visual stimulus onset. **(d)** All components, triggered on button presses.

a trigger. As shown in the overlay plots of the visual stimulus and button press triggered averages for *all* 122 SOBI components (Fig. 2cd), only a small fraction of the components showed task related responses, shown separately in Fig. 2ab.

The SOBI components can be displayed in the sensor domain by using the Neuromag software xfit (fullview). The sensor projections for two SOBI components are shown: one for a visual component (Fig. 3a) and the other for a right sensory-motor component (Fig. 3b). It is clear that the two SOBI components are projected selectively to sensors over the visual and right sensory-motor cortices. In contrast, the fullview plots of the sensor projections from the corresponding raw data (mixture of all components) have much wider distributions of sensor activtion (Fig. 3c,d).

In the following example, 122 SOBI components were separated from continuous 122-channel data collected during cognitive and simple sensory activation tasks (300 Hz and 600 Hz sampling rate respectively and band-pass filtered at 0.03–

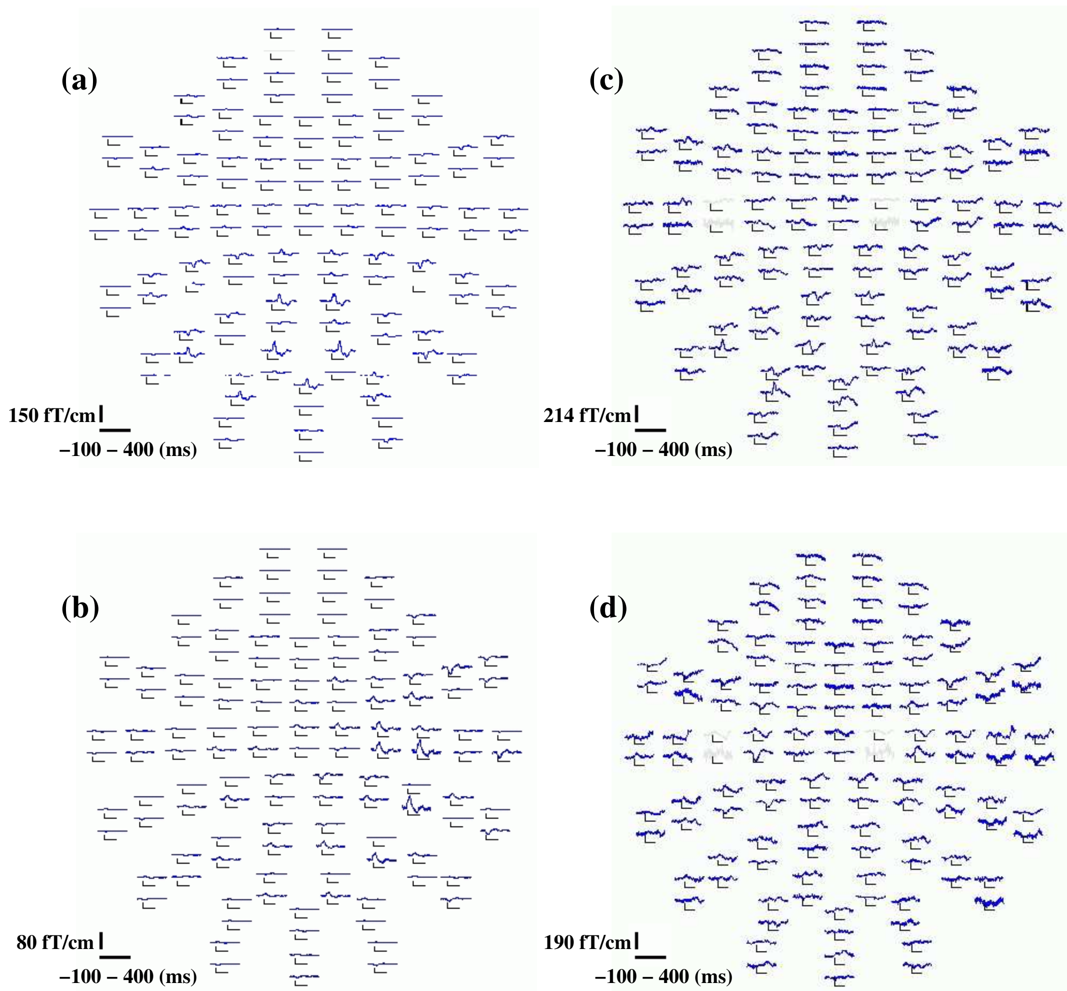

Figure 3: Sensor projections of SOBI components **(ab)** and of the mixed raw MEG data **(cd)** ($N = 90$ trials, **(ac)**: visual-stimulus-triggered; **(bd)**: button-press-triggered averages). **(a)** A SOBI component showing selective sensor activation over the occipito-parietal cortex. **(b)** A SOBI component showing selective activation over the right fronto-parietal cortex. **(c)** All components (unseparated data), triggered on visual stimulation. **(d)** All components (unseparated data), triggered on button presses. Aberrant sensors are shaded.

100 Hz).

3.1 SOBI Non-Neuronal Components

As illustrated in Fig. 1, MEG records magnetic signals associated with both noise and neuronal signals. These non-neuronal noise sources include ambient noises, such as 60hz or slow DC drift, ocular artifacts related signals, sensor jump related signals, and other unknown noise sources. Ocular artifacts were identified by the component's characteristic activation patterns in the field map and large amplitude responses in the MEG image (Fig. 4a), which match responses in the EOG (not shown). In these particular experimenters, a motor response typically triggered an eye blink response. The 60 Hz source was identified by the component's clearly visible cyclic activity in the MEG images in Fig. 4b. Components corresponding to sensor jumps were easily identified by the single-sensor activation in the field maps and sometimes by high contrast lines or dots in the MEG images (Fig. 4c). DC drift can be identified in the MEG image by a change of color from one block of trials to another and sources associated with such drift tend to have a broad activation pattern in the scalp projection (data not shown, but see Tang et al. (2000a)).

3.2 SOBI Neuronal Components

Before one can localize a neuronal source or estimate its single-trial response onset times, neuronal sources must first be identified among all n separated components (n = number of sensors). The first step in identification is to compute various event-triggered averages for each of the n components, *e.g.* visual, auditory, or somatosensory stimulus-locked, or motor-response-locked averages. If a component unambiguously shows an event-triggered response in the average, it becomes a candidate for being a neuronal source.

To identify neuronal sources that are directly task-related, both temporal and spatial constraints are used. For a task related component, if its field map and time course were consistent with known neurophysiological and neuroanatomical facts, we considered it a neuronal component reflecting the activity of a neuronal generator. For example, if the field map of a component shows activation over the occipital cortex and the visual stimulus triggered average for this component contains an evoked response that peaks between 50–100ms, then it is considered to reflect the activity of a visual source in the occipital lobe.

Fig. 5a shows the stimulus or response triggered averages for the evoked visual, somatosensory, and auditory responses in three SOBI components. The field maps of these SOBI components (Fig. 5b) have activations over the occipital-parietal, parietal, and temporal lobes that correspond to the expected visual, somatosensory, and auditory activation. For more details on the interpretation of these components in relation to the cognitive tasks, see Tang et al. (2002a,b). For identification of

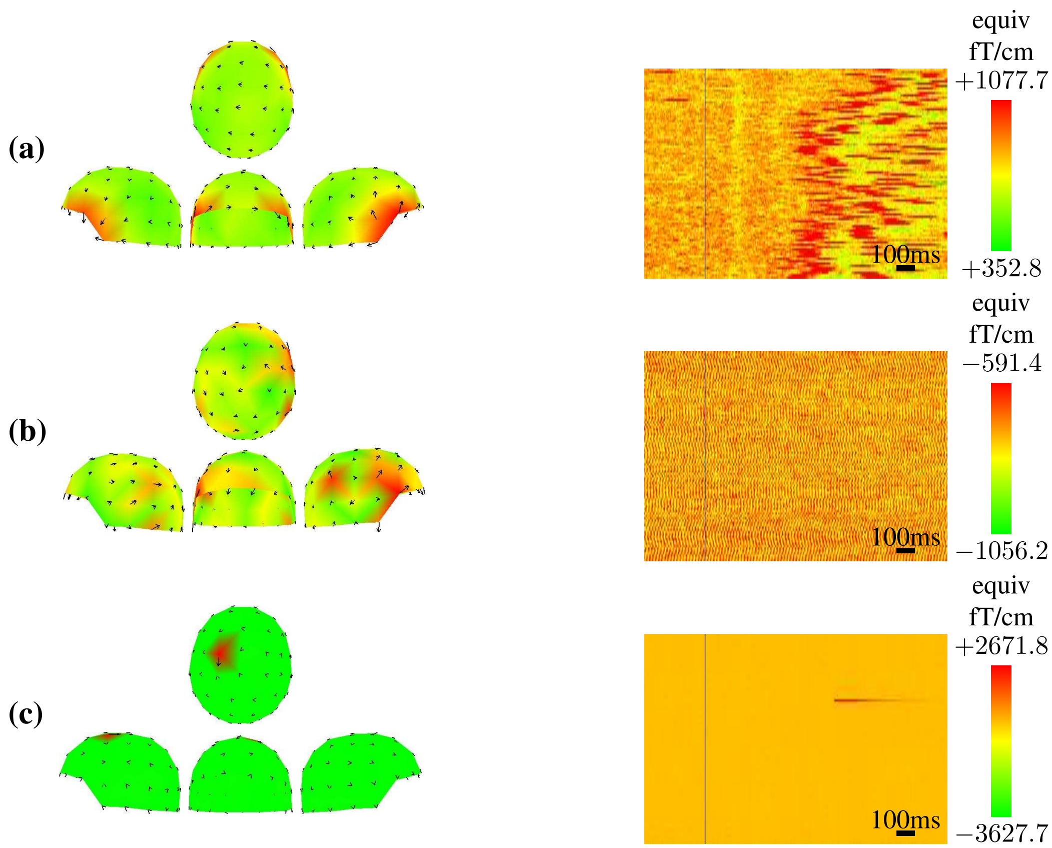

Figure 4: Field maps and unfiltered MEG images for **(a)** an ocular artifact component, **(b)** 60 Hz component, and **(c)** sensor jump component.

SOBI components within the same modality see Tang et al. (2000a).

4 Localization of SOBI Components

For the identified SOBI neuronal components, equivalent current dipoles can be fitted using the field maps as inputs to any source localization algorithm. As defined in Sec. 1.1, $\mathbf{W}$ is the estimated unmixing matrix, the estimated time courses for the sources are $\hat{\mathbf{s}}(t) = \mathbf{W}\,\mathbf{x}(t)$, and the corresponding estimated mixing matrix is $\hat{\mathbf{A}} = \mathbf{W}^{-1}$. Using these, the sensor signals resulting from just one of the components can be computed as $\hat{\mathbf{x}}(t) = \hat{\mathbf{A}}\,\mathbf{D}\,\mathbf{W}\,\mathbf{x}(t) = \hat{\mathbf{A}}\,\mathbf{D}\,\hat{\mathbf{s}}(t)$, where $\mathbf{D}$ is a matrix of zeros except for ones on the diagonal entries corresponding to each component which is to be retained. To localize a single SOBI component, one computes

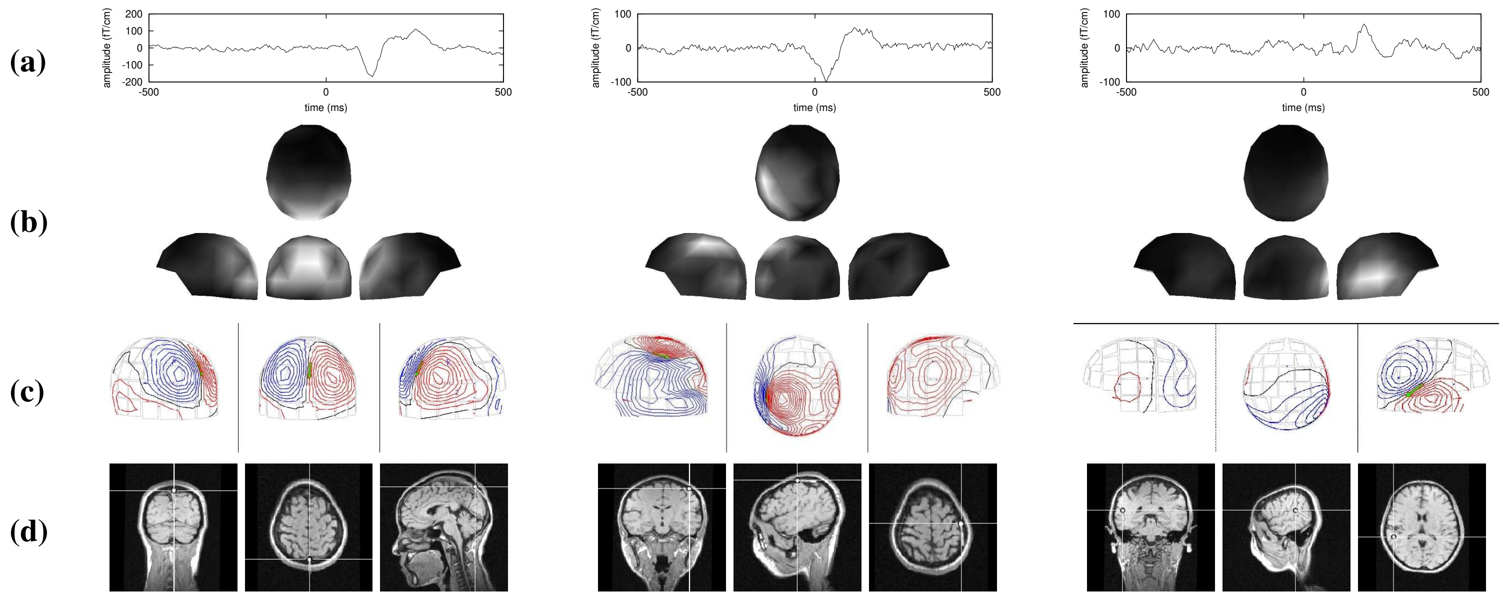

Figure 5: Examples of SOBI separated visual **(left)**, somatosensory **(middle)**, and auditory **(right)** components, shown in **(a)** event triggered averages ($N = 90$ trials), **(b)** field maps, **(c)** contour plot, and **(d)** the fitted dipole superimposed on the subject's own MRI. All sensors (channels) were used in generating the contour plots and fitting the dipoles.

$$\hat{\mathbf{x}}^{(i)}(t) = \hat{s}_i(t)\,\hat{\mathbf{a}}^{(i)} \tag{2}$$

where $\hat{\mathbf{a}}^{(i)}$ is the i^{th} column of $\hat{\mathbf{A}}$ and $\hat{\mathbf{x}}^{(i)}(t)$ is the sensor-space image of source i. Because $\hat{\mathbf{x}}^{(i)}(t)$ is at each point in time equal to the unchanging vector $\hat{\mathbf{a}}^{(i)}$, scaled by the time course $\hat{s}_i(t)$, dipole fitting algorithms will localize $\hat{\mathbf{x}}^{(i)}(t)$ to the same location no matter what window in time is chosen.

Theoretically, one sampling point in time across all sensors contains all information about the source. In practice, Neuromag software needs a time series of at least several samples. Therefore, we calculated the event-locked average for the component of interest and made a .fif file containing such averages for the dipole fitting algorithm.

4.1 Localization Across Multiple Modalities

The process of localizing SOBI components is simple. For each components of interest, we compute its sensor projections as above and we repackage a .fif file for the Neuromag dipole fitting software. One can select any time during the average time window to fit the dipole because the dipole solution is invariant to time. In contrast, when localizing sources directly from the mixed sensor data, the resulting dipole solution is sensitive to the dipole fitting time. The independence of SOBI localization from time selection can significantly simplify the dipole localization process by reducing the subjective input needed during time selection.

The contour plots of the visual, somatosensory, and auditory components and their corresponding dipole locations are shown in Fig. 5cd. These SOBI components have naturally dipolar contour plots without channel selection or reduction. Without SOBI pre-processing, in order to obtain dipolar field patterns, manually selecting a subset of channels (20-30) or exclusion of channels is often needed when modeling dipole sources from the mixed sensor data. Using SOBI pre-processing, we can remove this subjective step from the localization process.

Localization results shown in Fig. 5cd can be obtained directly from fitting dipoles to the field maps by a naive user who simply follows instructions without selecting dipole fitting time and without selecting channels.

4.2 Cross-Task and Cross-Subject Reproducibility

To show how reproducible the localization of SOBI components can be *across the four cognitive tasks,* we examined SOBI separated visual components from one subject. Across four tasks, the two occipito-parietal visual sources can be reliably localized within the same subjects for two SOBI separated components (Fig. 6cd).

For both visual sources, the time course of the response is highly repeatable across multiple tasks, as shown in the overlay plot (Fig. 6ab). The earlier visual responses were almost identical in both amplitude and response latency, (Fig. 6a) while the later responses varied only in amplitude across tasks (Fig. 6b). These visual SOBI components were localized to similar locations within the occipital and parietal lobes, as shown in Fig. 6c,d, in which fitted dipoles from multiple experiments are superimposed on the subject's own structural MRI. Notice that, in the field map, the right side of the head is shown on the right whereas in the MRI image, following radiological convention, the right is shown on the left.

To show how reproducible the localization of SOBI components can be *across subjects,* we examined SOBI separated somatosensory components from three subjects.[3] In all three subjects, we reliably identified two components (left and right) with button-press-locked responses in the somatosensory areas. Fig. 7 shows the time course, field map, contour plot, and fitted dipole for the SOBI somatosensory components in the right hemisphere of the three subjects. Notice the cross-subject similarity in the field maps, contour plots, and dipole locations (somatosensory cortex in the anterior parietal lobe, post-central sulcus).

4.3 Localization with and without SOBI

To offer quantitative comparison in the relative performance of source localization with and without SOBI, we attempted to identify and localize the most reliable occipito-parietal visual source, and both the left and right somatosensory sources in four subjects and four cognitive tasks[4] from SOBI components and from the unprocessed data. As all four tasks involved bilateral presentation of visual stimuli, we expected that at least one visual source would be found active in the occipito-parietal cortex. Similarly, because separate left and right button presses were required by all the tasks, we also expected that at least one left and one right somatosensory source would be active. For these *expected sources*, we attempted to localize the source with dipole fitting from SOBI components and from the raw sensor data (without SOBI). The percentage of the expected sources for which dipole solutions can be found are compared for localization with and without the aid of SOBI.

For a SOBI component to be considered a detectable neuronal source, there must be an evoked response that clearly deviates from the baseline in the averaged component data. We rejected all SOBI components with any ambiguity on this

[3]The fourth subject did right-hand index-mid finger button presses which differed from the rest of the subjects.

[4]For detailed description of the tasks, see Tang et al. (2002a,b)

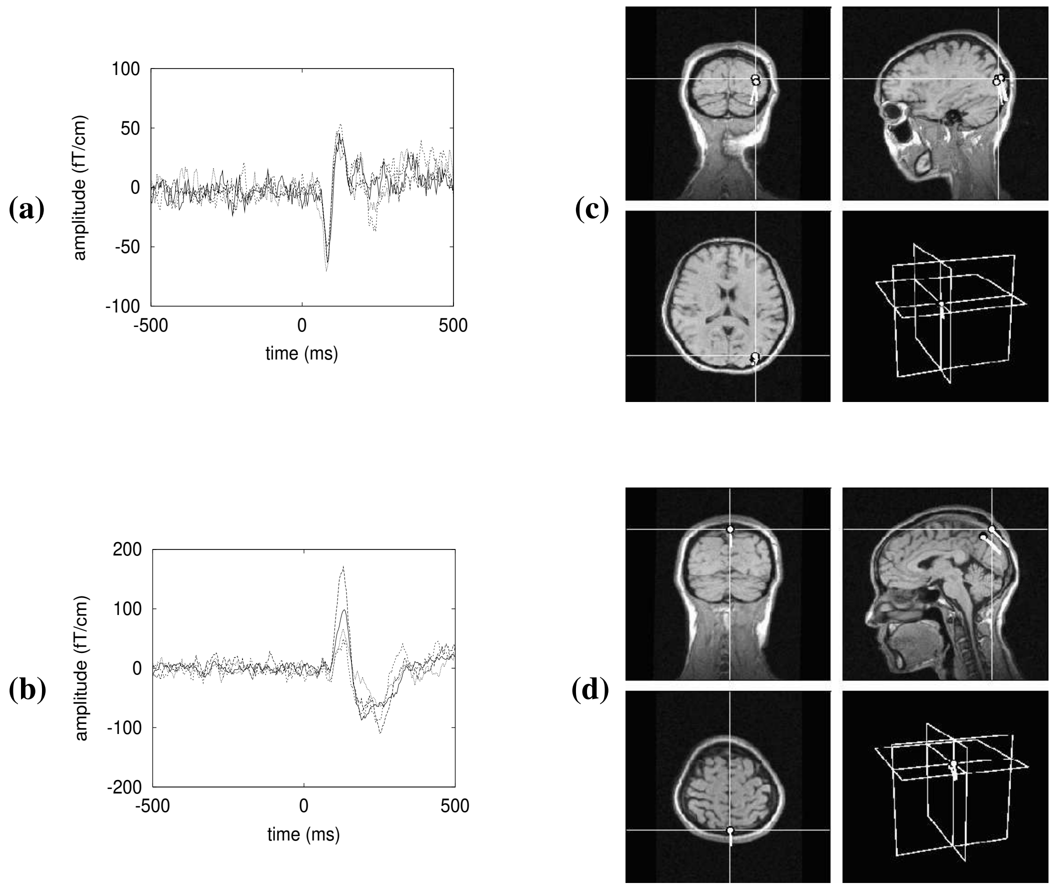

Figure 6: Cross-task consistency in the temporal profile **(ab)** and dipole location **(cd)** of two SOBI visual components. Occipital **(ac)** and occipito-parietal **(bd)** sources can be identified and localized consistently across multiple tasks (overlay). **(ab)** Visual stimulus-locked averages from 4 visual tasks, overlaid ($N = 90$ trials per task). **(cd)** Corresponding single ECDs for visual sources in **(ab)**. Notice consistency of the dipole locations across-tasks. Notice also the temporal profile of the earlier visual source **(a)** did not differ across tasks, but the amplitude of the later visual source **(c)** was modulated by the task conditions.

criterion. Secondly, the SOBI components must have a field map showing focal activation of sensors over the relevant brain regions (occipito-parietal cortex and anterior parietal cortex in this study). Thirdly, the contour plot for the SOBI component must be dipolar. Finally, the fitted dipole must be in the relevant cortical areas. For a source to be considered detectable using the conventional method of localization, one must first identify a sensor at which the largest evoked response is found. Secondly, the contour plot must be dipolar at the peak time. Finally, in

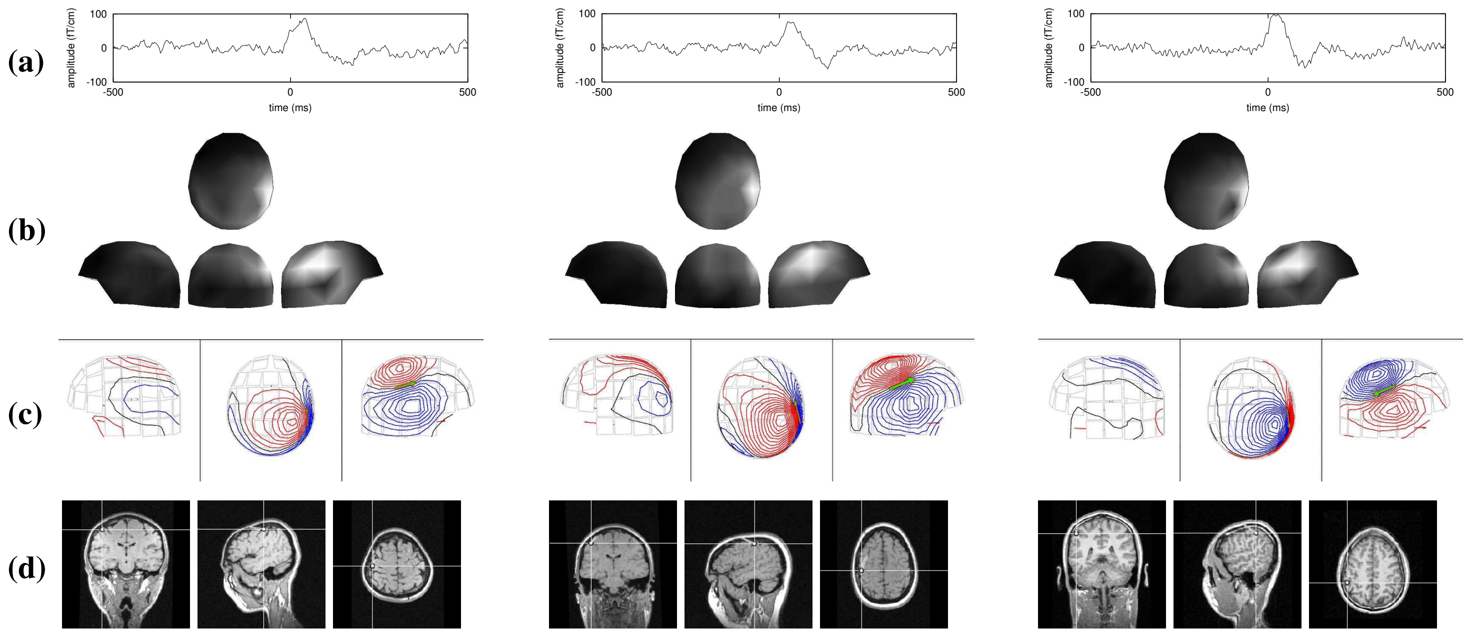

Figure 7: Somatosensory sources can be identified and localized consistently across multiple subjects (shown for the left source). Similar to Fig. 5 except the responses were locked onto the button press.

a few cases when multiple dipole solutions are needed, at least one of the dipoles is localized to the expected brain region. By allowing multiple dipole solutions for localization without SOBI pre-processing, our comparison biased against the SOBI method.

4.3.1 Visual Sources

Among all SOBI components, for each subject and each task, we were able to identify and localize an occipito-parietal visual source with a single dipole (100% detectability). These occipito-parietal components invariantly had very focal sensor projections, and the contour plots were invariantly dipolar even without channel selection (for example, see field map and contour plot in Fig. 5bc, left). A subset of channels over the occipito-parietal lobe (20–30 channels) were used for the purpose of fair comparison with the conventional analysis method without the aid of SOBI. The peak response latencies of these SOBI components ($N = 16$) were 139.0±7.6 and the dipole coordinates (X,Y,Z) were 7.5±2.6, −49.4±3.2, and 68.6±3.4 mm.

Using the conventional method of source localization directly from the unseparated sensor data, dipoles were fitted using the same or similar subset of channels selected over the occipito-parietal cortex. In all subjects and all tasks, the conventional method identified and localized at least one visual source in the occipito-parietal lobe (100% detectability). Of a total of 16 expected sources (4 tasks by 4 subjects), 10 could be fitted with a single dipole, 4 were fitted with two-dipole solutions, 1 was fitted with a three-dipole solution, and 1 was fitted with a four-dipole solution. When multiple dipole solutions were needed, at least one of them was localized to the occipito-pariental cortex. This variation in dipole solutions may reflect some individual differences in visual processing occurring outside of the occipito-parietal cortex. The peak response latencies of these occipito-pariental visual sources ($N = 16$) were 143.6±5.5 and the dipole coordinates (X,Y,Z) were 4.21±4.8, −55.89±2.68, and 59.42±3.83 mm.

4.3.2 Somatosensory Sources

For each subject and each task, with only two failures we were able to identify and localize 22 out of the 24 expected left and right somatosensory sources with a single dipole from SOBI components (3 subjects by 4 tasks by 2 hemispheres). All 22 somatosensory components invariantly had very focal sensor projections (see field maps) and the contour plots were invariantly dipolar even without channel selection (for example, see field map and contour plot in Fig. 7bc.) Single dipoles were fitted for these components, with a subset of channels over the somatosensory cortex (20–30 channels) selected for the purpose of fair comparison with the conventional analysis method. The peak response latencies were 33.3±4.2 and 30.8±3.4 ms for the left ($N = 11$) and right ($N = 11$) somatosensory sources. The dipole coordinates (X,Y,Z) were −39.4±2.4, 7.8±2.7, and 84.6±1.7 for the left and 45.69±2.1, 5.6±2.2, and 84.1±3.1 for the right somatosensory sources.

Using the conventional method of source localization directly from the unseparated sensor data, dipoles were fitted using the same or similar subset of channels selected over the somatosensory cortex. Of 24 sources expected, in 7 cases, no visible peak response could be identified in any of the sensors. Of the remaining 17 cases in which peak responses could be found in at least one sensor over the somatosensory cortex, 4 did not have dipolar fields, and 4 resulted in dipole locations outside of the head or in the auditory cortex. Single dipole solutions were found in only 9 cases. The peak response latencies of these somatosensory sources were 24.8±2.5 for the left hemisphere ($N = 5$) and 31.6±1.8 for the right hemisphere ($N = 4$). The dipole coordinates (X,Y,Z) were −43.3±3.9, 12.1±5.6, and 82.8±3.8 for the left 42.3±5.5, 15.9±2.7 and 89.9±1.4 for the right sources.

4.3.3 Statistical Comparisons

There was no significant differences in the detectability for the occipito-parietal source measured with and without SOBI. In both cases, 100% detectability (16 out of 16 expected sources) was found. In contrast, SOBI resulted in an increase in the detectability of the expected somatosensory sources (22 out of 24 for SOBI and 9 out of 24 for unprocessed data; χ^2 test $p < .0001$) (Fig. 8). The peak response latencies for the visual and somatosensory sources did not differ significantly when measured using and without using SOBI. For the visual sources, the precise dipole locations estimated with and without SOBI did not differ in the X and Y dimensions but nearly differed significantly in the Z dimension ($p = 0.05$). For the somatosensory sources, the precise dipole locations differed significantly in the Y dimension ($p < 0.05$) for the left source and in Y and Z dimensions for the right source ($p < 0.05$). As the true accuracy of source locations cannot be determined from these experiments without a depth-electrode, no quantitative comparisons can be made concerning accuracy.

4.4 SOBI Reduced Subjectivity and Labor

Because each component has a fixed field map, the dipole fitting solutions for SOBI components were neither sensitive to the time at which the dipoles were fitted nor to the sensor used for determining the time of fit. Within this map, each sensor reading reflects only activation due to a single source generator, or several temporally coherent generators as opposed to activation due to a combination of multiple

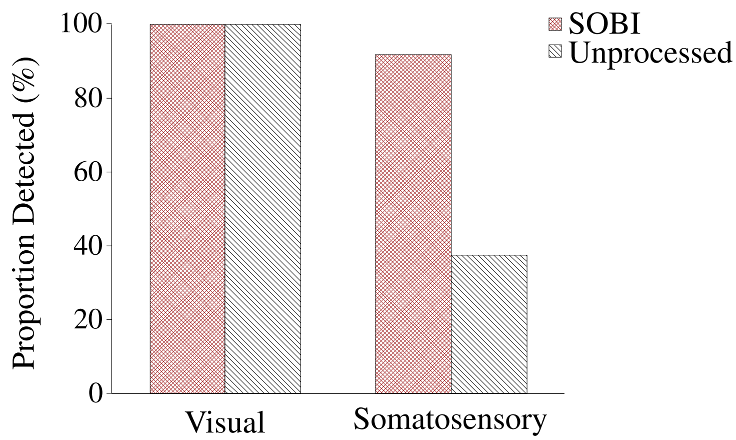

Figure 8: SOBI increased the detectability of expected neuronal sources for the more variable somatosensory activation.

generators, each with a different time course. Therefore, using SOBI, there is no need to subjectively select a time from a sensor for dipole fitting. One way to view the difference between dipole localization with and without SOBI processing is to view SOBI as an automatic and objective tool that allows the isolation of sensor activation due to an already isolated functionally independent generator. Secondly, simple SOBI components, which have field activation over early sensory processing areas, were almost always dipolar even without channel selection/reduction.[5] Using the Neuromag software, one can simply load in the average sensor signals for a given component and hit the fit button to get the dipole solution. The reduced subjectivity and time required to find dipole solutions can make data analysis and training of new researchers for MEG more cost-effective.

4.5 SOBI Improved Detectability of Neuronal Sources

SOBI separation of the data resulted in a greater detectability of somatosensory sources, but did not increase the detectability of visual sources. This modality-specific improvement in source detectability depended on the S/N ratio in the sensor data. Given this specific set of experiments, visual responses could be clearly identified from the raw sensor data even without the aid of SOBI, there was no room for further improvement in detectability by SOBI. In contrast, the relatively poor S/N ratio in the raw sensor data for the somatosensory responses caused many

[5]SOBI also separated out many complex components which have multiple patches or very board field activation. These components reflect synchronized activation in multiple brains. Functional connectivity may be inferred among these brain regions.

failures in identifying a sensor at which a peak response could be found and in determining the peak response time. Under this poor signal to noise condition, in all but two cases, SOBI resulted in components with the characteristic field map, characteristic temporal response profile, and the correct dipole location for a somatosensory source. These findings suggest another advantage that ICA algorithms can offer: improving the ability to detect and localize neuronal sources that are otherwise difficult to detect or are undetectable under relatively poor signal-to-noise conditions.

This improvement has significant practical implications. First, brain regions involved in higher level cognitive processing tend to show greater trial-to-trial variability in their activation, and therefore, have a lower signal-to-noise ratio in the average response. Second, behavioral tasks that bear greater resemblance to real world situations tend to involve greater variability in both stimulus presentation and subsequent processing. Finally, studies of clinical patients and children are often limited by the length of the experiment, and therefore, often provide data from a limited number of trials. Our results suggest that ICA may offer an improved capability in detecting and localizing neuronal source activations in these difficult situations.

It should be mentioned that fICA-separated components have been shown to yield localization results qualitatively similar to those arrived at without ICA preprocessing (Vigário et al., 1999). It may appear from this study that no substantial benefits from ICA could be found for neuromagnetic source localization. The experiment in this study was optimally designed to produce strong and focal activation of a small number of neuromagnetic sources and the S/N was high. Under such an optimal condition, the advantages of ICA algorithms are likely to be masked by a ceiling effect.

4.6 Summary

We identified and localized visual and somatosensory sources activated in four subjects during four cognitive tasks. Due to the relatively large variability involved in highly cognitive tasks and the small number of trials collected, these tasks were characterized by relatively poor signal-to-noise ratios in the sensor data and therefore were ideal for evaluating differential localization performance. Our results showed that despite the large variability associated with the visual and somatosensory activations during these particular tasks, SOBI was able to separate and identify visual and somatosensory components that were localized to expected cortical regions. Most importantly, for the most variable somatosensory activation evoked by incidental stimulation during button presses, SOBI pre-processing resulted in a greater rate of detection and localization for the expected somatosensory sources than that obtained from localization using the raw sensor data. Furthermore, the process of generating dipole solutions for SOBI components was simpler, more efficient, and less subjective.

5 Single-Trial Response Onset Time Detection

Single-trial response onset time detection is performed only when there is an evoked response that clearly deviates from the baseline in the averaged component data. For all identified neuronal sources, we estimated response onset times by the leading edge of the response, rather than the time of the peak response. This measure is more robust against noise and also better captures the intuitive goal of detecting the time of the earliest detectable response, rather than of the maximal response.

The process of single-trial response onset detection is iterative: both the threshold and detection windows are adjusted until no further reduction in false detection can be achieved. An initial threshold was set between the peak amplitude and one-half of the peak amplitude in the event triggered average plot (not shown). The beginning of the detection window initially was set at the time the event triggered averages first exceeded the range of baseline fluctuation. Typically, the baseline window is approximately 100 ms to 200 ms prior to stimulus onset. The detection window ended when the event triggered averages first returned to the same level as when the detection window began. (These initial values are not critical because they will be adjusted in both directions as described below.)

Because single-trial responses can be very different from the event triggered averages, the threshold and detection windows were adjusted through an iterative process to ensure that no responses were excluded. Using the initial threshold and detection window, response onset times were determined and graphically superimposed on the MEG image (detected response time (DRT) curve) to allow visual verification of the detected onset times. Because the detection windows should be sufficiently large to capture the entire distribution of response onset times, the DRT curve should be smooth. When multiple events were detected exactly at the begining of the detection window, it is most likely that the signal amplitude of the component has crossed the threshold *before* the begining of the detection window. Therefore, these events were considered false detections and were not marked by (or removed from) the DRT curve. For components showing biphasic responses, most of the single-trial response time analysis presented here was performed on the initial phase of the response, when the amplitude of the initial response was sufficiently large. Some results on the later phases are shown when the early phase response had such low amplitude as to make them difficult to detect using the method presented here.

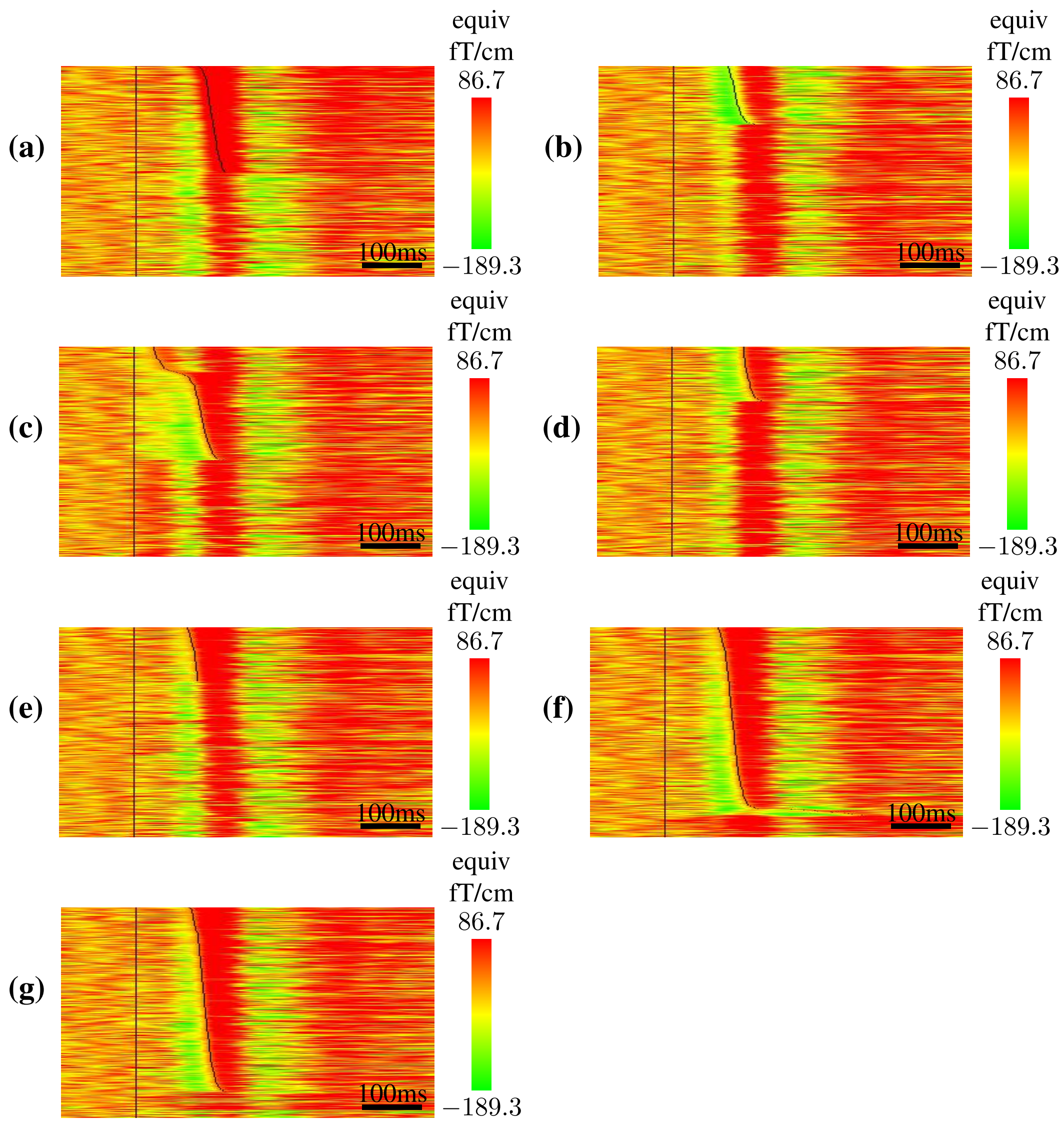

Figure 9: Examples, all from the same source, of sub-optimal detection due to **(a)** too high a threshold; **(b)** too low a threshold; **(c)** an early window beginning w_b; **(d)** a late window beginning w_b; **(e)** an early window end w_e; and **(f)** a late window end w_e. In **(g)** we show an optimal detection. See Table 1 for associated detection parameters and results.

5.1 Threshold

If the threshold is set too high not only can many trials remain undetected, but one will also overestimate the onset times by missing the initial onset. Overestimation

Cases	Detection Parameters			Detection Result	
	Threshold (fT/cm)	w_b (ms)	w_e (ms)	**Rate**	**Quality**
high threshold	150	70	120	177/350	missing onsets
low threshold	-100	70	120	97/350	missing onsets
early w_b	10	25	120	189/350	missing & false onsets
late w_b	10	95	120	91/350	missing onsets
early w_e	10	70	85	90/350	missing onsets
late w_e	10	70	320	313/350	false onsets
optimal	10	70	120	305/350	

Table 1: Detection parameters (threshold and detection window) and detection results for the examples given in Fig 9. Thresholds are relative to a per-trial 100 ms pre-stimulus baseline.

of onset times is easily seen as a right shift in the DRT curve from the leading edge of color change associated with the responses (Fig. 9a). Because the threshold is set too high, many single-trial responses were missed (detection rate: 177/350). Because all trials with responses detected are displayed on top of the MEG image and sorted by detected response latency, and trials with no responses detected are displayed at the bottom, missing responses are apparent under visual inspection as shown at the bottom of Fig. 9a. If the threshold is set too low, false detection can occur when the amplitude of baseline fluctuation is relatively large. In this case, many false detections would be made at the begining of the detection window (253/350), resulting in a low detection rate (97/350) as shown in Fig. 9b. In both cases, the threshold could be either lowered or raised accordingly in the next iteration until the DRT curves captures the edge of the color change associated with the apparent response onset times.

5.2 Detection Window

Once the detection threshold is determined, one further examines the MEG image for false detections associated with incorrect settings of the beginning and ending of the detection window, w_b and w_e. If w_b is too early, the response window will include a part of the baseline. As a result, the DRT curve shows a discontinuity, with the point of discontinuity separating trials of false detection (left portion) from trials of correct detection (right portion), as in Fig. 9c. If w_b is too late, many single-trial responses would be detected at a time *later* than the time when the signal amplitude first crosses the threshold. These false detections were made exactly at the begining of the detection window. These false detections (246/350) were automatically removed from the DRT curves and the corresponding trials were displayed at the bottom portion of the MEG image (Fig. 9d).

If w_e is too early, later response onsets may be missing (see bottom portion of Fig. 9e). This case is apparent upon visual inspection. If w_e is too late, the later portion of a biphasic response will be falsely detected as the initial response. This form of false detection is easily seen near the tail end of the DRT curve (Fig. 9f) where initial responses were clearly missed, while the second phase of the responses were marked. In any of the above cases, one can adjust the detection window parameters for the next iteration.

For each neuronal component, this iterative process continues until no further reduction in the frequency of false detections or missing responses can be achieved. The final result is shown in Fig. 9g. Statistics on the detected onset times (mean$\pm$sem) are then computed and reported along with the resulting MEG image (Fig. 9g). The same procedure can be performed on a control window of equal size either prior to or following the actual detection window. The resulting number of detected onsets within the control windows can be compared statically with that obtained for the detection window.

5.3 Effect of Filter Length on Detected Onset Times

As filtering can affect response onset times, we first investigated the effect of a low-pass filter, as such a filter is often used to remove noise unrelated to the evoked responses. Fig. 10 and Fig. 11 display the result of response onset time detection using different low-pass filter parameters for a SOBI component with auditory evoked responses. Filtering visibly reduced the amount of background noise, thus highlighting the evoked responses (Fig. 10). There was no apparent change in the detected onset times or in the number of detections as the low-pass filter was changed from no filter, to 40 Hz, 20 Hz and 10 Hz (Fig. 10) and as the roll off parameter was changed from 0.5 Hz to 5 Hz (Fig. 11). A quantitative comparison between the detected onset times using different low-pass filter parameters revealed very small changes in the number of onsets detected. When a more aggressive low-pass filter was used, the number of events detected was reduced from to 145 to 141 (4 from a total of 150 trials).

If an onset time is only detectable when no filter is used, it is possible that such a detected response is a result of false detection due to noisy ongoing background activity. Therefore, by using a more aggressive low-pass filter, one can reduce the chance of false detection. On the other hand, a more aggressive filter can change the detected onset times. Thus, a change in the number of onsets detected caused by different low-pass filters could be a result of better onset time estimation associated with a reduction in false detection or worse estimation due to temporal smearing after filtering. To ensure that temporal smearing was not the cause of the change in the detected onset times, we always performed the detection procedure both with and without filtering, and examined graphically whether the filtering altered the temporal profile of the evoked response. As shown in Fig. 10, filtering with a 10 Hz low-pass filter changed the estimated onset times by less than 2 ms, and did not distort the profile of the evoked responses.

A more aggressive low-pass filter can reduce the influence of ongoing background activity, and thereby minimize false detection, without significantly altering the temporal profile of the evoked responses. Therefore, in the following analysis, a low-pass filter of 10 Hz with a roll off of 5 Hz was used unless otherwise specified. It is important to note that for different neuronal sources, the effect of a given filter on response onset times will be different. When a filter significantly changes the temporal profile of the evoked responses, a less aggressive filter should be used for an accurate estimation of response onsets.

5.4 Response Onset Time Detection Across Sensory Modalities

In this section we demonstrate that single-trial response onset time detection can be achieved in three major sensory modalities and under experimental conditions of both large and small trial-to-trial variability. Single-trial onset time detection with *large* trial-to-trial variability was performed for the visual and somatosensory evoked responses recorded during the four cognitive tasks. Single-trial onset time detection with *small* trial-to-trial variability was performed for the auditory evoked responses recorded during the simple binaural pure tone presentation.

The detected response onset times are shown in MEG images (Fig. 12b), with the evoked responses aligned to the stimulus onset (time zero, marked by the vertical line on the left side of the MEG image) and the detected response times marked as a curve to the right of the stimulus onset line (DRT curve). The detection results are shown sorted by latency from stimulus to detected response onset. The stimulus triggered average (Fig. 12a), sensor projections or field maps (Fig. 12c), and dipole location superimposed on the subject's structural MRI images (*e.g.* Fig. 12d) are also provided, for comparison with results from standard analysis. For the visual source shown in Fig. 12a-d, the single-trial response onsets were detected in 64 of 90 trials (71.1%). The estimated onset times were 111$\pm$1 ms. Its temporal profile in the average response, the field map, the contour plot, and the dipole location were characteristic of typical visual sources from the occipito-parietal lobes. For comparison with typical visually evoked responses, see Brenner et al. (1975); Hari (1994); Supek et al. (1999).

For the somatosensory source shown in Fig. 13a-f, the single-trial response on-

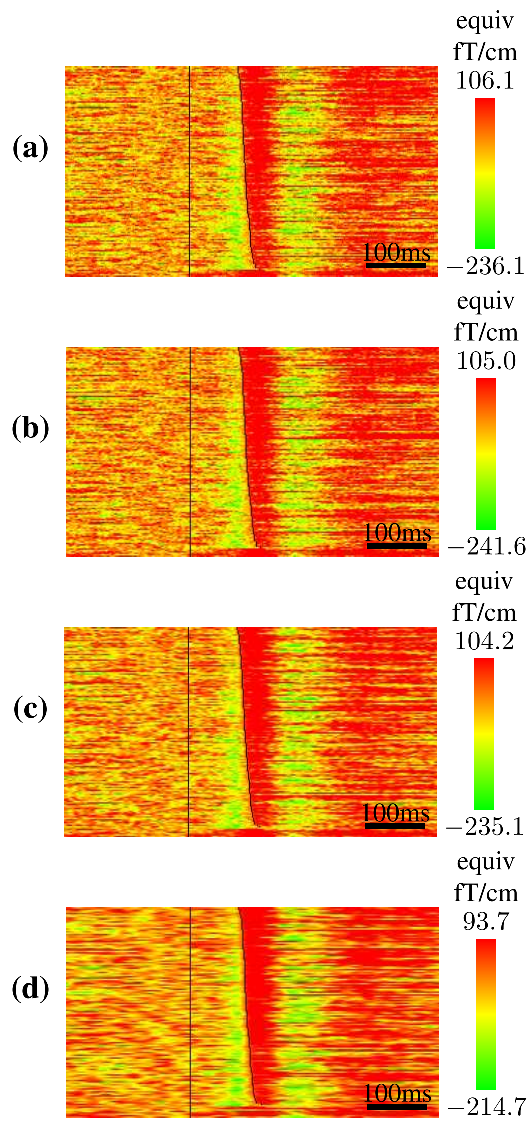

Figure 10: Effect of low-pass filter on response onset time detection (onset times, % response detected). **(a)** No filter: 90±1 ms; 96.7% **(b)** low-pass at 40 Hz: 91±1 ms; 96% **(c)** low-pass at 20 Hz: 92±1 ms; 95.3%. **(d)** low-pass at 10 Hz: 92±1 ms; 94%. For all panels, a roll-off of 5 Hz was used.

sets were detected in 129 of 150 trials (86%) when the contralateral thumb pressed the mouse button and in 105 of 120 trials (87.5%) when the ipsilateral thumb pressed the mouse button. The response onset times from the time when the button press was detected on the trigger line were -1 ± 2 ms and 15 ± 1 ms for the contra- and ipsilateral activation respectively. These numbers indicate that the somatosen-

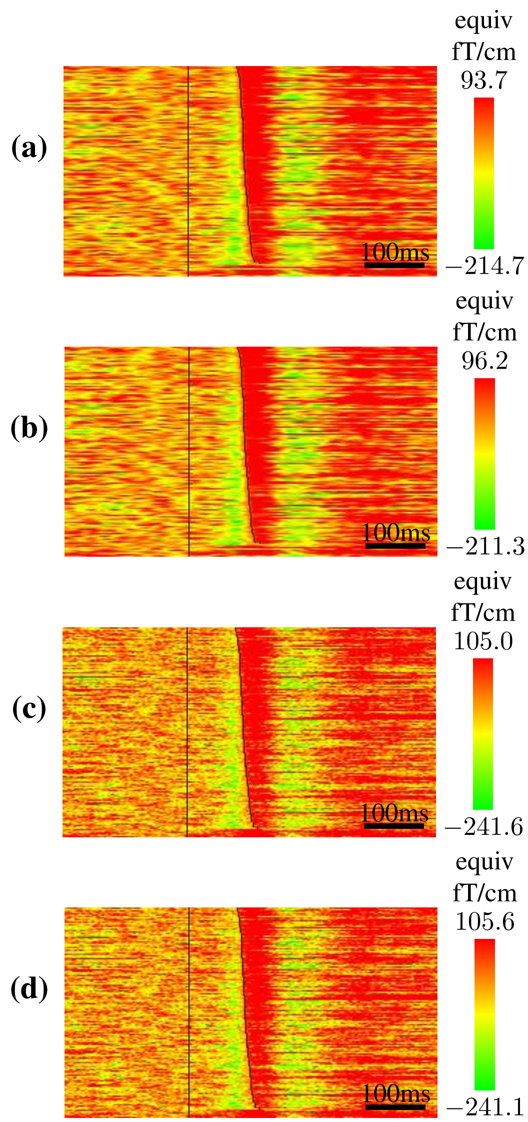

Figure 11: Effect of filter roll-off on response onset time detection (onset times, % response detected). **(a)** 10 Hz low-pass and 5 Hz roll-off: 92±1 ms, 94%. **(b)** 10 Hz low-pass and 0.5 Hz roll-off: 92±1 ms, 94%. **(c)** 40 Hz low-pass and 5 Hz roll-off: 91±1 ms, 96%. **(d)** 40 Hz low-pass and 0.5 Hz roll-off: 91±1 ms, 96%.

sory responses could start as soon as the thumb movement was initiated; as soon as, or even before, the mouse button was completely depressed. The temporal profile in the average responses was slower to rise and broader in width than the typical responses evoked by electrical stimulation (Brenner et al., 1978; Hari and Forss, 1999; Karhu and Tesche, 1999). This was expected because somatosensory stimulation due to button press movement and feedback is much more prolonged and variable than stimulation by the brief and well-controlled median nerve shock. The field map, contour plot, and dipole location are consistent with activation of the hand region of the somatosensory cortex.

For the auditory source shown in Fig. 14a-e, the single-trial response onsets were detected in 141 of 150 trials (94%). The estimated response onset times were 92±1 ms. The temporal profile in the average response, field map, contour plot, and dipole location were characteristic of typical auditory sources. This particular auditory SOBI component had a two-dipole solution, one in each of the two hemispheres, and (necessarily, due to the SOBI decomposition) both having the same time course of response. This is consistent with the binaural stimulation used in this experiment.[6] The temporal profile in the average response, the field map, the contour plot, and the dipole location were characteristic of typical auditory sources in the temporal lobes. For comparison with typical auditory evoked responses, see Hari et al. (1980); Romani et al. (1982); Roberts et al. (2000).

5.5 Cross-Subject Response Onset Detection: Visual

As previously discussed (Tang et al., 2000b, 2002a), visual sources were identifiable along both the ventral and dorsal streams. The occipito-parietal sources along the dorsal stream varied less in location and in response profile. In contrast, the occipito-temporal sources along the ventral stream showed greater variability in response profile and precise location. To give the readers a sense of how well the single-trial onset time detection procedure can perform across a variety of visual sources, we show detection for the visual responses from a variety of visual areas from multiple subjects.

In 13 of 16 (81%) expected visual sources along the ventral processing stream,[7] single-trial onset time detection could be performed. The detection rate was 71±2%, and the estimated response onset times were 133±5 ms ($N = 13$). Fig. 12e,f,g shows results of onset time detection for the visual sources from three additional subjects. Sources were chosen to reflect variability in the responses and in the detection.

[6] It is possible to obtain two separate components from the left and right hemisphere if there is sufficient hemispherical asymmetry in the temporal details of neuronal responses from the left and right auditory cortices.

[7] Given the tasks involved memory of visual forms, we expected at least one visual source to be activated along the ventral processing pathway. A total of 16 such sources are expected for 4 experiments in 4 subjects.

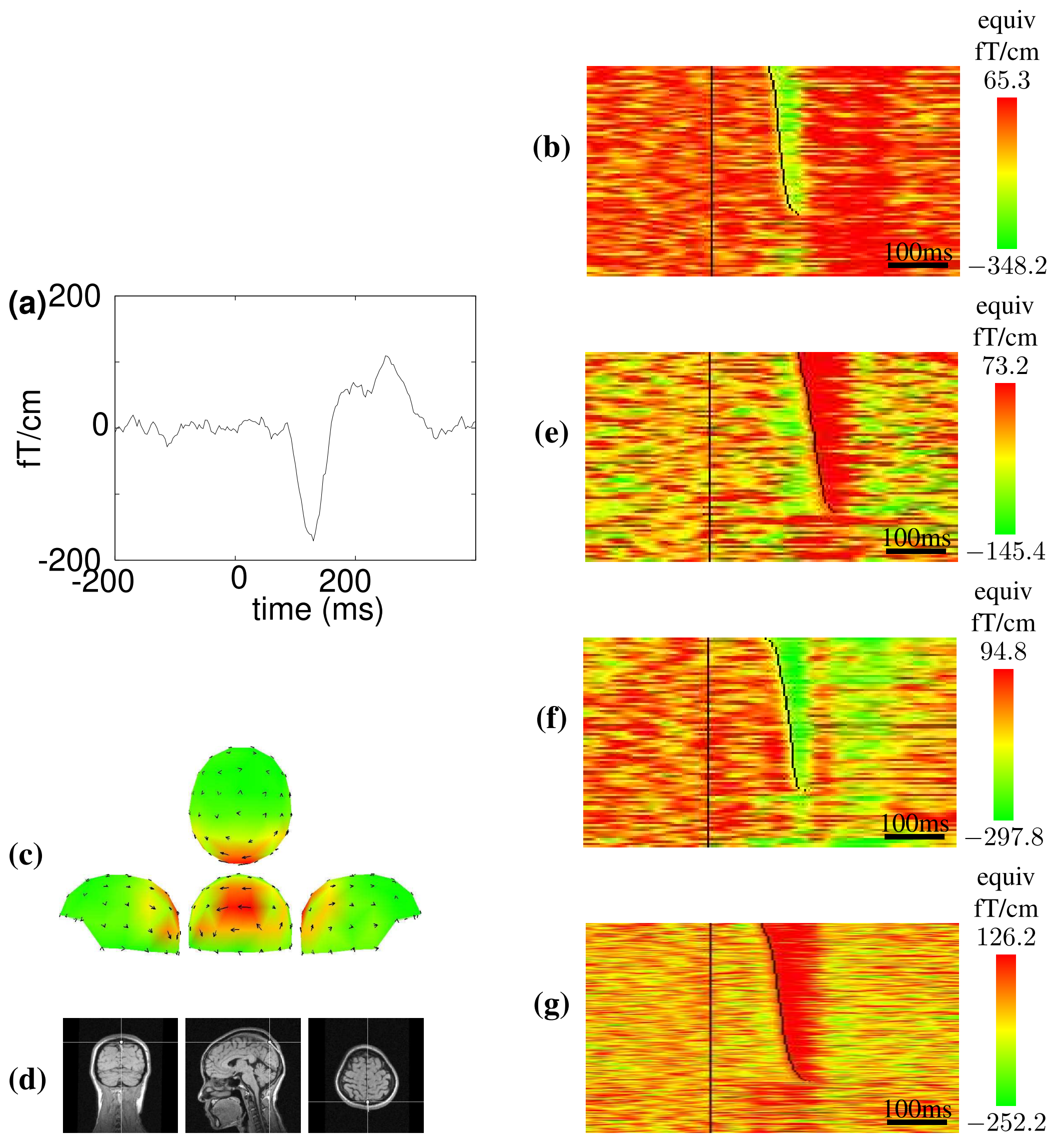

Figure 12: **(a)–(d)** Detection of single-trial response onset times from an occipito-parietal source that responded to a visual stimulus. **(a)** Visual stimulus triggered average response (unfiltered); **(b)** detected single-trial response times marked on an MEG image; **(c)** field map of the parietal source; **(d)** fitted ECD superimposed on the subject's structural MRI images. **(e)–(g)** Single-trial visual response onset detection in visual sources across three additional subjects, sorted by onset latency. **(b)**, **(e)–(g)**: subjects 1–4. $N = 90$ trials except for **(d)**, $N = 270$ trials.

5.6 Cross-Subject Response Onset Detection: Somatosensory

Somatosensory sources were identified in all subjects who made button press responses during the four cognitive tasks. Single-trial response onset time detection was attempted on one of the SOBI somatosensory components for each subject in at least one of the four tasks. Because the activation of these somatosensory sources was highly variable, in only 7 of 24 (29%) of the somatosensory sources could single-trial onset time detection be performed. Among these sources, for the contralateral button presses, single-trial onset times were estimated to be 0±3 ms with a detection rate of 81±2% ($N = 7$). For the ipsilateral button presses, single-trial onset times were estimated to be 5±3 ms with a detection rate of 76±5% ($N = 3$). Fig. 13g,h shows results of onset time detection for the latter source in two additional subjects.

5.7 Cross-Subject Response Onset Detection: Auditory

Auditory evoked responses from the presentation of a pure tone were the least variable in comparison to the above described visual and somatosensory responses from the cognitive tasks. In all six subjects, auditory sources can be identified and localized from the SOBI separated components. Single-trial response onset time detection could be performed in 6 of 6 expected auditory sources[8] with a detection rate of 80±5%, and estimated response onset times of 85±1 ms ($N = 6$).

Fig. 14f,g,h show results of onset detection for the auditory source from three additional subjects. As the trial-to-trial variability in auditory stimulation was very low in comparison to the variability in the visual and somatosensory stimulation during the cognitive tasks, the average detection rate was higher for these auditory sources. Furthermore, single-trial response onset time detection could be performed among a higher percentage of expected sources (100%) for the auditory responses than for the visual (81%) and somatosensory (29%) responses.

5.8 Statistical Analysis

To determine quantitatively whether the detected responses are due to to baseline ongoing activity, we performed the detection procedure on a baseline or control window of equal length immediately before or sometime after the response window defined by w_b and w_e, using otherwise identical parameters. When a post-response control window was selected, we made sure that the background fluctua-

[8]Given the tasks involved auditory stimulation, we expected at least one auditory sources to be activated in each subject. A total of 6 auditory sources are therefore expected for the 6 subjects.

tion was comparable to or greater than that of the pre-stimulus baseline. To determine whether the detected response onsets were more numerous than those detected in the control windows, we performed a t-test on the difference between the number of detections during the response window and the number of detections during the control windows. This test result ($t = 9.200, df = 16, p < 0.005$) indicates that our method is capable of detecting evoked responses from single-trial MEG data that is above background ongoing activity. Fig. 15 shows the result of response onset time detection for the response window, a pre-response control window, and a post-response control window. The trials are sorted according to the detected onset times in Fig. 15a,c,e and the same detection results are shown in chronological order in Fig. 15b,d,f.

For sources with good apparent signal to noise ratios across multiple subjects, we applied the detection procedure to both a detection window (w_b to w_e) and a control window. The detection rates for the response windows were $79 \pm 4\%$ ($N = 4$) for the somatosensory components, $65 \pm 3\%$ ($N = 7$) for the visual components, and $80 \pm 5\%$ ($N = 6$) for the auditory components. When all sources were pooled, the detection rate within the detection window across all modalities was $74 \pm 3\%$. The detection rates obtained for the control windows using otherwise identical parameters were much lower: $14 \pm 4\%$ for the somatosensory components, $37 \pm 3\%$ for the visual components, and $27 \pm 4\%$ for the auditory components. When all sources were pooled, the detection rate across all modalities within the control window was $28 \pm 3\%$. The ratio between the rate of detection for the response and control windows was 7.11 ± 1.82 for the somatosensory components, 1.84 ± 0.18 for the visual components, and 3.26 ± 0.41 for the auditory components. When all sources were pooled the ratio across all modalities was $3.58 \pm 0.66\%$.

Because these components were obtained during different experiments, a number of factors could contribute to the large variation, including differences in stimulus presentation, task complexity, different stages of processing (early *vs.* later), pathways (*e.g.* ventral vs dorsal), modalities of sensory processing (visual, auditory, and somatosensory), different states of alertness (amount of alpha oscillation), and different levels of power in the background brain activity. The detection for the visual components seemed to be particularly poor in comparison to those for the somatosensory and auditory components. It is important to point out that the visual components included here have a greater intrinsic variability due to the number of brain regions from which visual components can be localized, in comparison to the much more homogeneous source locations of the somatosensory and auditory components. In addition, the visual cortex tends to have more alpha band background activity than any of the other sensory cortices (Williamson et al., 1996). Greater alpha band background activity can contribute to the higher detection rate during the control window.

6 Discussion

We will conclude this chapter with a brief discussion of the independence assumption made by all ICA methods, a summary of state-of-art ICA capabilities, and an outline of future directions.

6.1 Assumptions

SOBI shares a number of weaknesses with all ICA methods: they all assume that there are as many sensors as sources; they all make some sort of independence assumption; they all assume that the mixing process is linear; and they all assume that the mixing process is stable. Here, we discuss assumptions of particular relevance to SOBI and MEG, rather than general issues in ICA. Like all ICA algorithms, SOBI assumes that the mixing process is stable. In the context of MEG, a stable mixing process corresponds to assuming that the head is motionless relative to the sensors. For this reason head stabilization can be particularly important in MEG when ICA is used. SOBI also assumes that there are at least as many sensors as sources. For us, this is not a serious problem, as our MEG device has 122 sensors, yet we recover only a few dozen sources that show task-related evoked responses. The observation that only a small number of sources are active during typical cognitive and sensory activation tasks is consistent with the results of studies using both EEG (Makeig et al., 1999) and MEG Vigário et al. (2000). The crucial assumption in ICA is that of independence. For a thorough discussion of the independence assumption as it pertains to MEG, see Vigário et al. (2000). Here, we will discuss independence only in the context of the particular measure of independence used by SOBI.

6.2 The SOBI Independence Assumption

The major concern that EEG and MEG researchers have with the independence assumption arises from the fact that if one computes correlations between EEG or MEG sensor readings over multiple brain regions during behavioral tasks, one would find that some brain regions have non-zero correlations. A good example of correlated brain activity is the apparently correlated evoked responses from neuronal populations in multiple visual areas along the processing pathway during a visual stimulus presentation. Based on such an observation, one could conclude that as the statistical independence assumed by ICA is clearly violated, the results of ICA must not be trusted. Yet, we have shown that SOBI was able to separate visual components that clearly correspond to neuronal responses from early and later visual processing stages that are correlated due to common input (Tang et al., 2000b). Others (Makeig et al., 1999; Vigário et al., 2000) have produced behaviorally and neurophysiologically meaningful components under a variety of task conditions.

As different ICA algorithms use the independence assumption differently, we offer the following explanation that applies specifically to SOBI. One needs to recognize that correlation is not a binary quantity. Consequently, neither is violation of the independence assumption. The important question is not whether the assumption is violated but whether the assumption is *sufficiently* violated such that the estimated neuronal sources by SOBI are no longer meaningful. The way SOBI uses the independence assumption is to minimize the total correlations computed with a set of time delays. As such, each delay-correlation matrix $\mathbf{R}_\tau$ generally makes only a small contribution to the objective function. For example, the correlation one would observe between V1 and V2 responses could be high only at or around one particular time delay, say in $\mathbf{R}_{20\mathrm{ms}}$. In optimizing its objective function, SOBI can leave a particularly large non-zero off-diagonal element, say the one corresponding to the 20 ms delayed correlation between V1 and V2, in order to minimize the sum squared off-diagonal elements across all the components and time delays. Therefore, this particular method of maximizing independence is not necessarily incompatible with a large correlation at a particular time delay between two sources sharing common inputs.

Most ICA algorithms, including SOBI, minimize some objective function. It is possible for the optimization process to find a poor local minimum. In general, poor results can result from many underlying causes: poor experimental design, poorly conducted experiments, poor head stabilization, poor optimization within the ICA algorithm, violation of assumptions, etc. No amount of attention to any one possible problem can validate ICA-based methods for processing functional brain imaging data. As with any statistical procedure, the real issue here should not be whether assumptions are violated at all, but whether the algorithms can robustly produce components that are behaviorally, neuroanatomically, and physiologically interpretable, despite some violation of the assumptions under which the algorithms were derived. For example, t-tests are very robust against the violation of normality assumption and are therefore regularly performed on data which are not guaranteed to be Gaussian. Only empirical results can give confidence that a method is correctly separating the MEG data.

6.3 ICA Advantages

Applying SOBI, one particular ICA algorithm to data from a total of 10 subjects (four tested on four cognitive tasks and six from one auditory sensory activation task), we provided step-by-step demonstration of how to apply ICA to MEG data, how to identify neuromagnetic sources of interest, how to localize the identified sources, and how to measure single-trial response onset times from the identified neuronal sources. Through this process, we have demonstrated that ICA offers:

- automatic separation of neuronal sources from noise sources (ocular artifacts, 60 Hz, and sensor noise);
- automatic separation of neuronal sources from different modalities (visual, somatosensory, and auditory);
- automatic separation of neuronal sources within the same sensory modality (left and right somatosensory sources);
- reduction in subjectivity and simplification of the source modeling process (no need to set the dipole fitting time and or to select channels);
- increased probability of neuronal source detection and localization under poor S/N conditions;
- over 90% detection rate in single-trial response onset time measurement.

6.4 Future Directions

A number of important methodological issues remain. The first concerns with the effect of varying the delays used in the calculation of the correlation matrix and the interaction between the selection of delays and the temporal property of the neuronal source activation. The second concerns with the amount of the data needed for good separation results. The third has to do with how SOBI may interface with other source modeling method to generate the best localization results. The last but perhaps the most urgent one is to develop softwares systems that integrate the above outlined analysis steps in a seamless fashion to support users with a wide range of computer experience.

References

Aine, C., Huang, M., Stephen, J., and Christner, R. (2000). Multistart algorithms for MEG empirical data analysis reliably characterize locations and time courses of multiple sources. *Neuroimage*, 12(2):159–172.

Amari, S.-I. and Cichocki, A. (1998). Adaptive blind signal processing—neural network approaches. *Proceedings of the IEEE*, 9.

Bell, A. J. and Sejnowski, T. J. (1995). An information-maximization approach to blind separation and blind deconvolution. *Neural Computation*, 7(6):1129–1159.

Belouchrani, A., Meraim, K. A., Cardoso, J.-F., and Moulines, E. (1993). Second-order blind separation of correlated sources. In *Proc. Int. Conf. on Digital Sig. Proc.*, pages 346–351, Cyprus.

Brenner, D., Lipton, J., Kaufman, L., and Williamson, S. J. (1978). Somatically evoked magnetic fields of the human brain. *Science*, 199:81–83.

Brenner, D., Williamson, S. J., and Kaufman, L. (1975). Visually evoked magnetic fields of the human brain. *Science*, 190:480–482.

Cao, J. T., Murata, N., Amari, S., Cichocki, A., Takeda, T., Endo, H., and Harada, N. (2000). Single-trial magnetoencephalographic data decomposition and localization based on independent component analysis approach. *IEICE Transactions on Fundamentals of Electronics, Communications and Computer Sciences*, E83A(9):1757–1766.

Cardoso, J.-F. (1994). On the performance of orthogonal source separation algorithms. In *European Signal Processing Conference*, pages 776–779, Edinburgh.

Cardoso, J.-F. (1998). Blind signal separation: statistical principles. *Proceedings of the IEEE*, 9(10):2009–2025.

Comon, P. (1994). Independent component analysis: A new concept. *Signal Processing*, 36:287–314.

Ermer, J. J., Mosher, J. C., Huang, M. X., and Leahy, R. M. (2000). Paired MEG data set source localization using recursively applied and projected (RAP) MUSIC. *IEEE Transactions on Biomedical Engineering*, 47(9):1248–1260.

Hari, R. (1994). Human cortical functions revealed by magnetoencephalography. *Prog. Brain Res.*, 100:163–168.

Hari, R., Aittoniemi, K., Jarvinen, M.-L., and Varpula, T. (1980). Auditory evoked transient and sustained magnetic fields of the human brain. *Exp. Brain Res.*, 40:237–240.

Hari, R. and Forss, N. (1999). Magnetoencephalography in the study of human somatosensory cortical processing. *Phil. Trans. R. Soc. Lond. B*, 354:1145–1154.

Hotelling, H. (1933). Analysis of a complex of statistical variables into principal components. *Journal of Educational Psychology*, 24:417–441, 498–520.

Huang, M. X., Aine, C., Davis, L., Butman, J., Christner, R., Weisend, M., Stephen, J., Meyer, J., Silveri, J., Herman, M., and Lee, R. R. (2000). Sources on the anterior and posterior banks of the central sulcus identified from magnetic somatosensory evoked responses using multi-start spatio-temporal localization. *Human Brain Mapping*, 11(2):59–76.

Hyvärinen, A. (1999). Survey on independent component analysis. *Neural Computing Surveys*, 2:94–128.

Hyvärinen, A. and Oja, E. (1997). A fast fixed-point algorithm for independent component analysis. *Neural Computation*, 9(7).

Ioannides, A. A., Liu, M. J., Liu, L. C., Bamidis, P. D., Hellstrand, E., and Stephan, K. M. (1995). Magnetic-field tomography of cortical and deep processes: examples of real-time mapping of averaged and single trial MEG signals. *Inter. J. of Psychophysiol.*, 20(3):161–175.

Jung, T.-P., Humphries, C., Lee, T.-W., Makeig, S., McKeown, M. J., Iragui, V., and Sejnowski, T. J. (1999a). Removing electroencephalographic artifacts: comparison between ICA and PCA. In *Neural Networks for Signal Processing VIII*. IEEE Press.

Jung, T.-P., Humphries, C., Lee, T.-W., McKeown, M. J., Iragui, V., Makeig, S., and Sejnowski, T. J. (2000a). Removing electroencephalographic artifacts by blind source separation. *Psychophysiology*, 37:163–178.

Jung, T.-P., Makeig, S., Westerfield, M., Townsend, J., Courchesne, E., and Sejnowski, T. J. (1999b). Analyzing and visualizing single-trial event-related potentials. In *Advances in Neural Information Processing Systems 11*, pages 118–124. MIT Press.

Jung, T.-P., Makeig, S., Westerfield, M., Townsend, J., Courchesne, E., and Sejnowski, T. J. (2000b). Removal of eye activity artifacts from visual event-related potentials in normal and clinical subjects. *Clinical Neurophysiology*, 111(10):1745–1758.

Karhu, J. and Tesche, C. D. (1999). Simultaneous early processing of sensory input in human primary (SI) and secondary (SII) somatosensory cortices. *J. Neurophysiol.*, 81:2017–2025.

Kinouchi, Y., Ohara, G., Nagashino, H., Soga, T., Shichijo, F., and Matsumoto, K. (1996). Dipole source localization of MEG by BP neural networks. *Brain Topogr.*, 8(3):317–321.

Lewine, J. D. and Orrison, II, W. W. (1995). Magnetoencephalography and magnetic source imaging. In Orrison, II, W. W., Lewine, J. D., Sanders, J. A., and Hartshorne, M. F., editors, *Functional Brain Imaging*, pages 369–417. Mosby, St. Louis.

Makeig, S., Bell, A. J., Jung, T.-P., and Sejnowski, T. J. (1996). Independent component analysis of electroencephalographic data. In *Advances in Neural Information Processing Systems 8*, pages 145–151. MIT Press.

Makeig, S., Jung, T. P., Bell, A. J., Ghahremani, D., and Sejnowski, T. J. (1997). Blind separation of auditory event-related brain responses into independent components. *Proc. Natl. Acad. Sci. USA*, 94(20):10979–10984.

Makeig, S., Westerfield, M., Jung, T.-P., Covington, J., Townsend, J., Sejnwoski, T. J., and Courchesne, E. (1999). Functionally independent components of the late positive event-related potential during visual spatial attention. *J. Neurosci.*, 19(7):2665–2680.

Mosher, J. C. and Leahy, R. M. (1998). Recursive music: A framework for EEG and MEG source localization. *IEEE Transactions on Biomedical Engineering*, 45(11):1342–1354.

Mosher, J. C. and Leahy, R. M. (1999). Source localization using recursively applied projected (RAP) MUSIC. *IEEE Transactions on Signal Processing*, 47(2):332–340.

Mosher, J. C., Lewis, P. S., and Leahy, R. M. (1992). Multiple dipole modeling and localization from spatiotemporal MEG data. *IEEE Transactions on Biomedical Engineering*, 39(6):541–557.

Nagano, T., Ohno, Y., Uesugi, N., Ikeda, H., Ishiyama, A., and Kasai, N. (1998). Multi-source localization by genetic algorithm using MEG. *IEEE Transactions on Magnetics*, 34(5/pt.1):2976–2979.

Roberts, T., Ferrari, P., Stufflebeam, S., and Poeppel, D. (2000). Latency of the auditory evoked neuromagnetic field components: Stimulus dependence and insights toward perception. *J Clin Neurophysiol.*, 17(2):114–129.

Romani, G., Williamson, S., and Kaufman, L. (1982). Tonotopic organization of the human auditory cortex. *Science*, 216(4552):1339–40.

Schmidt, D. M., George, J. S., and Wood, C. C. (1999). Bayesian inference applied to the electromagnetic inverse problem. *Human Brain Mapping*, 7(3):195–212.

Schwartz, D. P., Badier, J. M., Bihoue, P., and Bouliou, A. (1999). Evaluation of a new MEG–EEG spatio-temporal localization approach using a realistic source model. *Brain Topogr.*, 11(4):279–289.

Sekihara, K., Nagarajan, S. S., Poeppel, D., Miyauchi, S., Fujimaki, N., Koizumi, H., and Miyashita, Y. (2000). Estimating neural sources from each time-frequency component of magnetoencephalographic data. *IEEE Transactions on*

Biomedical Engineering, 47(5):642–653.

Sekihara, K., Poeppel, D., Marantz, A., Koizumi, H., and Miyashita, Y. (1997). Noise covariance incorporated MEG-MUSIC algorithm: A method for multiple-dipole estimation tolerant of the influence of background brain activity. *IEEE Transactions on Biomedical Engineering*, 44(9):839–847.

Supek, S., Aine, C. J., Ranken, D., Best, E., Flynn, E. R., and Wood, C. C. (1999). Single vs. paired visual stimulation: superposition of early neuromagnetic responses and retinotopy in extrastriate cortex in humans. *Brain Res.*, 830(1):43–55.

Tang, A. C., Pearlmutter, B. A., Malaszenko, N. A., Phung, D. B., and Reeb, B. C. (2002a). Independent components of magnetoencephalography: Localization. *Neural Computation*, 14(8):1827–1858.

Tang, A. C., Pearlmutter, B. A., Phung, D. B., and Malaszenko, N. A. (2002b). Independent components of magnetoencephalography: Single-trial response onset times. *Neuroimage*.

Tang, A. C., Pearlmutter, B. A., Zibulevsky, M., and Carter, S. A. (2000a). Blind separation of multichannel neuromagnetic responses. *Neurocomputing*, 32–33:1115–1120.

Tang, A. C., Pearlmutter, B. A., Zibulevsky, M., Hely, T. A., and Weisend, M. P. (2000b). An MEG study of response latency and variability in the human visual system during a visual-motor integration task. In *Advances in Neural Information Processing Systems 12*, pages 185–191. MIT Press.

Tang, A. C., Phung, D., Pearlmutter, B. A., and Christner, R. (2000c). Localization of independent components from magnetoencephalography. In *International Workshop on Independent Component Analysis and Blind Signal Separation*, pages 387–392, Helsinki, Finland.

Uutela, K., Hämäläinen, M., and Salmelin, R. (1998). Global optimization in the localization of neuromagnetic sources. *IEEE Transactions on Biomedical Engineering*, 45(6):716–723.

Vigário, R., Jousmäki, V., Hämäläinen, M., Hari, R., and Oja, E. (1998). Independent component analysis for identification of artifacts in magnetoencephalographic recordings. In *Advances in Neural Information Processing Systems 10*, pages 229–235. MIT Press.

Vigário, R., Särelä, J., Jousmäki, V., Hämäläinen, M., and Oja, E. (2000). Independent component approach to the analysis of EEG and MEG recordings. *IEEE Transactions on Biomedical Engineering*, 47(5):589–593.

Vigário, R., Särelä, J., Jousmaki, V., and Oja, E. (1999). Independent component analysis in decomposition of auditory and somatosensory evoked fields. In *Proc. First International Conference on Independent Component Analysis and Blind Source Separation ICA'99*, pages 167–172, Aussois, France.

Williamson, S., Kaufman, L., Curtis, S., Lu, Z., Michel, C., and Wang, J. (1996). Neural substrates of working memories are revealed magnetically by the local suppresson of alpha rhythm. *Electroencephalogr Clin Neurophysiol Suppl*, 47:163–180.

Wübbeler, G., Ziehe, A., Mackert, B.-M., Müller, K.-R., Trahms, L., and Curio, G. (2000). Independent component analysis of non-invasively recorded cortical magnetic DC-fields in humans. *IEEE Transactions on Biomedical Engineering*, 47(5):594–599.

Ziehe, A., Müller, K.-R., Nolte, G., Mackert, B.-M., and Curio, G. (2000). Artifact reduction in magnetoneurography based on time-delayed second order correlations. *IEEE Transactions on Biomedical Engineering*, 47(1):75–87.

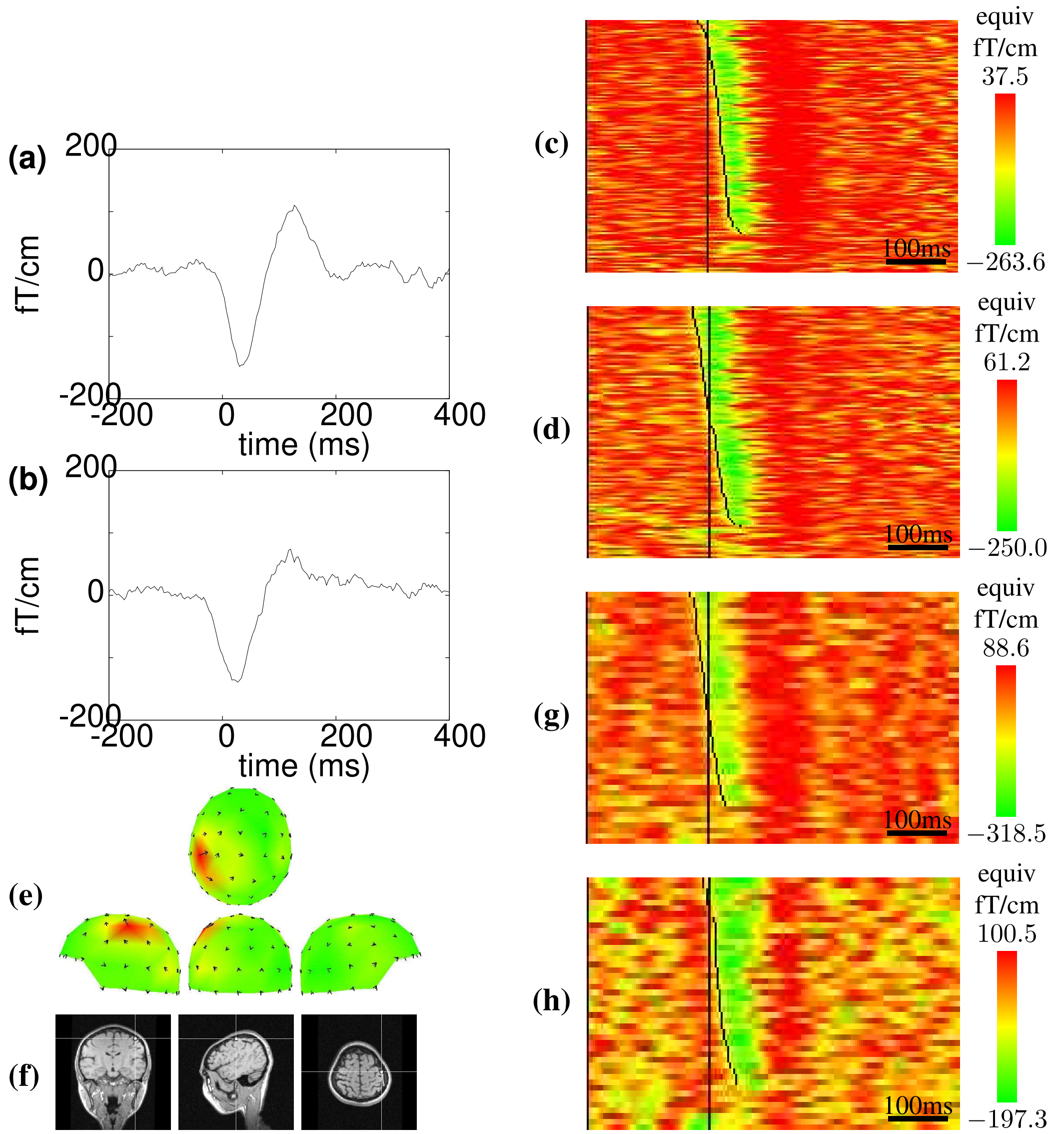

Figure 13: Detection of single-trial response onset times from a somatosensory (SS) source that responded to left **(a)** and right **(b)** button presses. **(a)**/**(b)** Left and right button press triggered average responses (unfiltered). **(c)**/**(d)** Detected single-trial response onset times triggered by left and right button presses respectively, marked on MEG images; **(e)** field map of the somatosensory source; **(f)** fitted ECD superimposed on the subject's structural MRI images. **(g)**/**(h)** Single-trial somatosensory response onset detection across two additional subjects, sorted by onset latency. **(c)**/**(g)**/**(h)**: subjects 1–3. Shown for contralateral activation only. The number of trials varied from subject to subject.

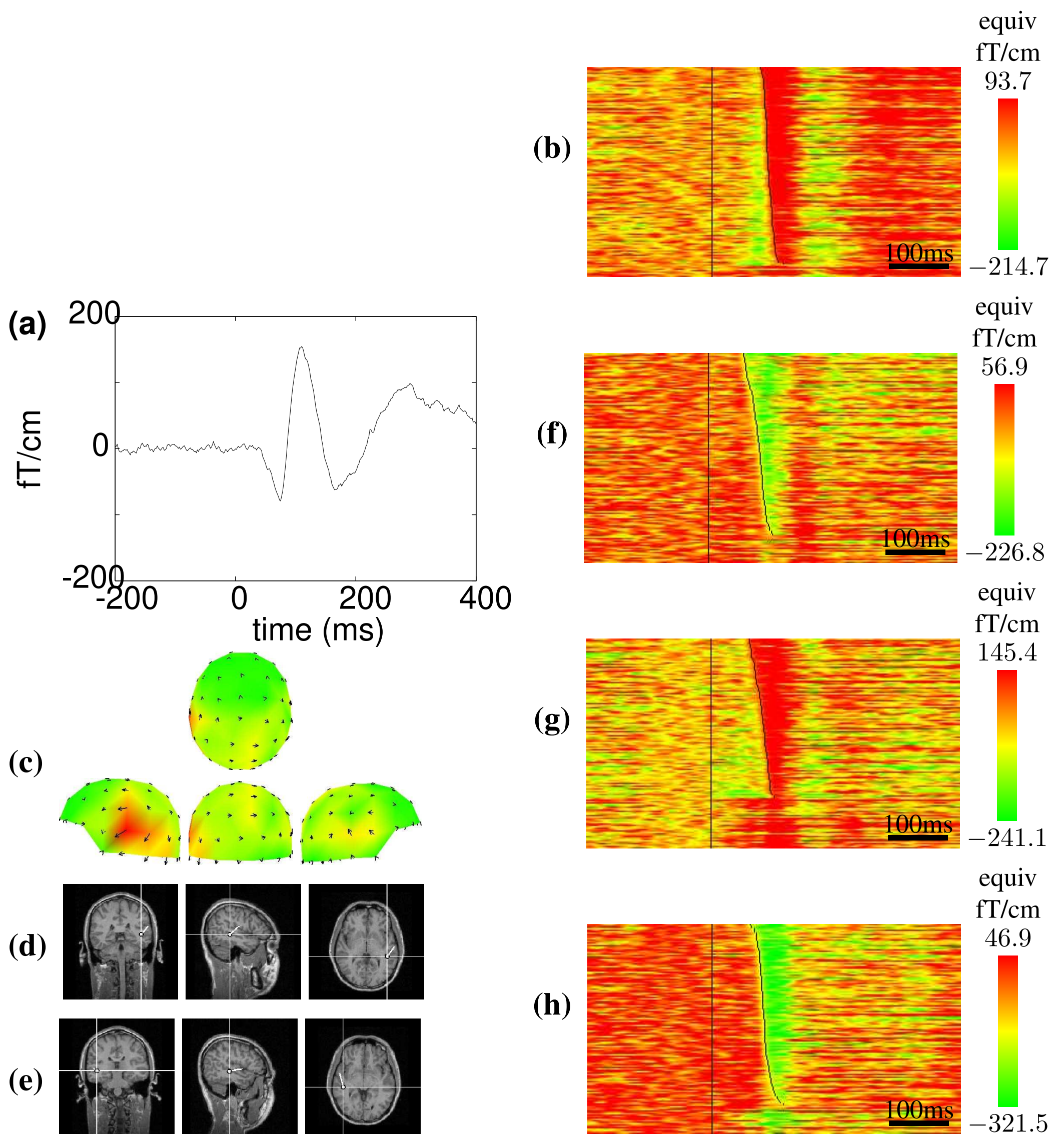

Figure 14: Detection of single-trial response onset times from an auditory source. **(a)** Auditory stimulus triggered average response (unfiltered). **(b)** Detected single-trial response times marked on an MEG image. **(c)** Field map of the temporal source. **(d)**/**(e)** Fitted ECD superimposed on the subject's structural MRI images. **(f)**–**(h)** Single-trial auditory response onset detection across three additional subjects, sorted by onset latency. **(b)**, **(f)**–**(h)**: subjects 1–4. $N = 150$ trials.

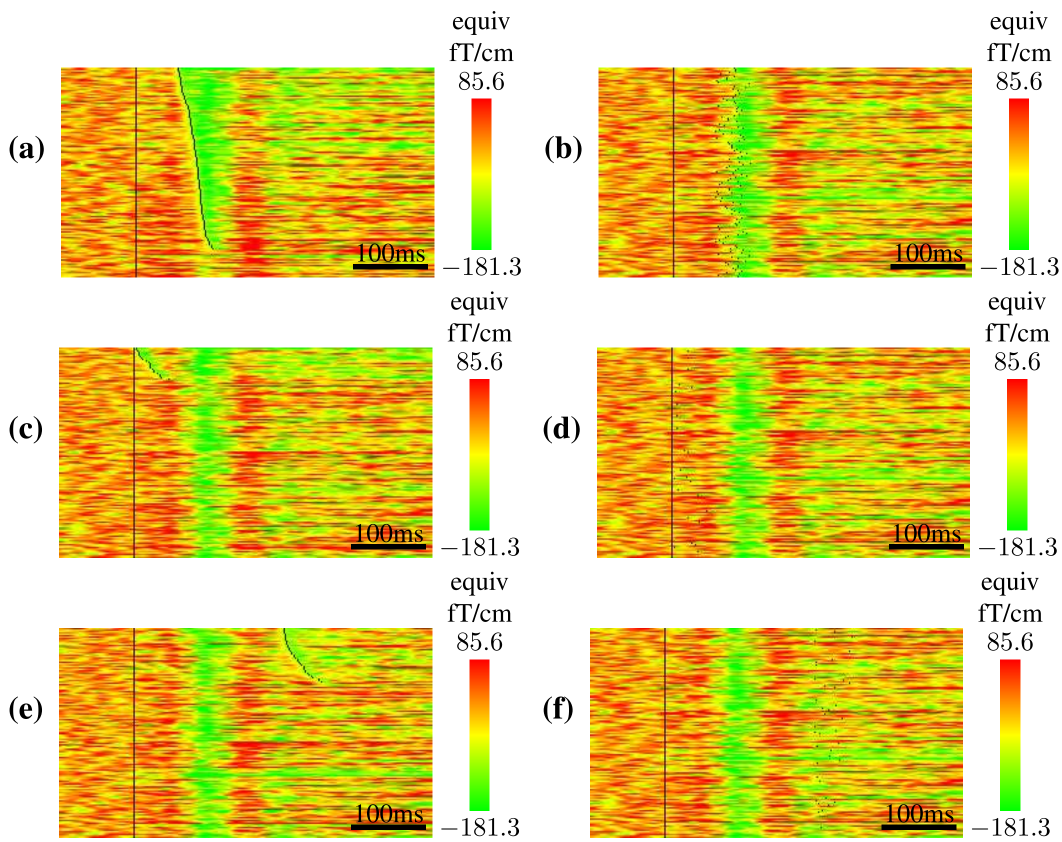

Figure 15: Detected response onsets for the response and pre- and post-response control windows, in **(a)** response window, sorted; **(b)** response window, unsorted; **(c)** pre-control window, sorted; **(d)** pre-control window, unsorted; **(e)** post-control window, sorted; **(f)** post-control window, unsorted.